Clemson University
TigerPrints

All Theses | Theses

12-2023

Converging Human Intelligence With AI Systems to Advance Flood Evacuation Decision Making

Rishav Karanjit
rkaranj@clemson.edu

Follow this and additional works at: https://tigerprints.clemson.edu/all_theses

Recommended Citation

Karanjit, Rishav, "Converging Human Intelligence With AI Systems to Advance Flood Evacuation Decision Making" (2023). *All Theses*. 4185.
https://tigerprints.clemson.edu/all_theses/4185

This Thesis is brought to you for free and open access by the Theses at TigerPrints. It has been accepted for inclusion in All Theses by an authorized administrator of TigerPrints. For more information, please contact kokeefe@clemson.edu.

CONVERGING HUMAN INTELLIGENCE WITH AI SYSTEMS TO ADVANCE FLOOD EVACUATION DECISION MAKING

A Dissertation
Presented to
the Graduate School of
Clemson University

In Partial Fulfillment
of the Requirements for the Degree
Master of Science
Computer Science

---

by
Rishav Karanjit
December 2023

Accepted by:
Dr. Nathan McNeese, Committee Chair
Dr. Vidya Samadi, Co-chair
Dr. Feng Luo, Committee Member

ABSTRACT

The powers that artificial intelligence (AI) has developed are astounding, with recent success in integrating into a human cognitive workflow. AI will attain its full potential only if, as part of its intelligence, it also actively teams up with humans to co-create solutions. Combining AI simulation with human understanding and strategic abilities through data convergence may optimize the process and provide a capacity akin to "teaming intelligence." This thesis will introduce the concepts of Human AI Convergence (HAC) capabilities for flood evacuation decision-making. The concept introduced in this thesis is the first step toward the HAC concept in weather disaster applications. This research demonstrates a synergy between humans and AI by integrating the data produced by humans through social media with an AI system to enhance a flood evacuation decision-making problem. The prediction from Long short-term memory (LSTM) and a river hydraulic model, i.e., Height Above Nearest Drainage (HAND), is integrated with human data from X (previously Twitter) to visualize flood inundation areas, which acts as a 3rd party agent for a HAC system. The goal is to synthesize and analyze HAC competence in flood evacuation emergency management and harness the full potential of AI as a partner in real-time planning and decision-making. This thesis has explored why HAC intelligence is essential to emergency planning and decision-making, providing a general structure for researchers to use HAC to devise effective systems that cooperate well and evaluate state-of-the-art, and, in doing so, providing a research agenda and a roadmap for future flood evacuation emergency management, rescue, and decision

making. This state-of-the-art flood evacuation product stands to advance the frontier of human-AI collaborative research significantly.

Keywords: Artificial Intelligence; Human-AI Convergence; Flood Emergency Management; Evacuation Decision Making and Planning.

DEDICATION

To my parents and brother

To Dr. Vidya Samadi and my thesis committee

To my team at Hydroinformatics and Hydroresources Research (HHR) Lab at Clemson University

To everyone who has been a part of this journey

ACKNOWLEDGMENTS

I want to thank my committee, Dr. Vidya Samadi, Dr. Nathan McNeese, and Dr. Feng Luo. This research is supported by the U.S. National Science Foundation (NSF) Directorate for Engineering under grant CMMI 2125283. NSF is acknowledged for its generous allotment of cloud computing resources through the Advanced Cyberinfrastructure Coordination Ecosystem: Services & Support (ACCESS) program. Clemson University is acknowledged for its generous allotment of computing time on the Palmetto cluster.

TABLE OF CONTENTS

Page

Table of Contents (Continued) Page

LIST OF TABLES

LIST OF FIGURES

CHAPTER ONE

INTRODUCTION

Imagine a Category 5 storm slams a coastal region, batters the area with a powerful combination of wind and rain and keeps lashing buildings, businesses, and infrastructure with severe storm surges, powerful winds, and inland flooding. The bridges and roads become inaccessible, the power lines are damaged, the airports stay inoperable, and the region's residents are forced to fend for themselves until assistance arrives. This situation is the vivid and ominous picture that many tropical cyclones create. The situation is complex and frightening – yet it has become a new norm for many coastal regions worldwide. To find a proper solution, emergency management officials must reconcile the enormous demands these occurrences place on the infrastructure of service delivery and decision-making processes in the communities they impact. [1].

To maintain tabs on all the various issues, a collaborative human and artificial intelligence (AI) teaming intelligence can emerge as a beacon capable of comprehensively evaluating the multifaceted implications of a given course of action. Incredibly, a teammate has a special knack for considering all the ramifications of a plan of action [2]. This partnership will facilitate the model's recollection of numerous things, including prior emergency restrictions, locations of vital emergency supplies, evacuation routes, and social issues. Indeed, this model’s response to disaster events can improve physical, cognitive, and social capabilities to dynamically adapt to changes, predict the environment, and

acquire knowledge through experience and interactions with human teammates [3]. By combining the data of humans and AI, novel tools can be developed to empower the AI system to acquire the ability to collaborate on action, context, and "intelligence" during weather emergency decision-making processes.

On the other hand, with human-AI collaboration, humans can perform tasks such as search and rescue, communication, and emotional support, which require human empathy and social skills. In contrast, AI can perform flood forecasting for evacuation decision-making tasks. The proposed collaboration model places significant emphasis on the tight coordination between human agents and AI systems. This cooperation is driven by a shared objective, which necessitates the exchange of crucial information through diverse forms of communication, prediction, and the achievement of high-level coordination tasks. [4]. Previous Human-AI convergence (HAC) studies have primarily focused on the interaction and effectiveness of human teams with AI in robotic swarms [2], landed aircraft perimeter security [5], protection behaviors in collaborative games [6], and how various factors (e.g., communication, a person's understanding of the limits or mistakes an AI system might make) affect team performance in a HAC implementation [7] [8].

Evacuation is crucial for minimizing the risk of injury or loss of life during extreme events. However, the decision to evacuate can be complex, involving multiple factors. AI has recently become a viable solution in flood evacuation. AI machines can collaborate

with humans to improve decision-making when dealing with time-critical/real-time disasters, large datasets, and analytical problems. The approach to uniting data from humans and AI leverages the strengths of humans and AI systems, resulting in more efficient and effective flood evacuation processes. The tasks performed by AI in flood evacuation require large amounts of data processing, analytics, and decision-making, which can be overwhelming for humans.

An intricate strategy is proposed within flood prediction and disaster management, capitalizing on the potential of state-of-the-art technologies and diverse data sources. This tool utilizes gauge height values as a critical input for predicting impending flooding events, facilitated by the prowess of machine learning models, including techniques such as Recurrent Neural Networks (RNNs) designed to capture temporal dependencies in data. By establishing a connection between historical gauge height readings and subsequent flood occurrences, these models can offer valuable insights into the dynamic patterns of river behavior, aiding in the anticipation of flood surges. Further enhancing the accuracy of flood assessment, integrating predicted gauge heights with flood inundation mapping emerges as a significant advancement. In addition, river hydraulic techniques, such as "Height Above Nearest Drainage (HAND)," can be employed to visualize the potential areas vulnerable to inundation. By merging this model with forecasted gauge heights, a comprehensive depiction of flood extents materializes, allowing decision-makers to anticipate the impact on specific geographical locations and critical infrastructure.

Moreover, integrating transportation data proves valuable to bolster the precision of emergency response strategies. This data provides insights into the geospatial distribution of road networks, critical access points, and potential bottlenecks, offering a comprehensive view of the region's transport infrastructure. Integrating transportation geospatial data with flood predictions enables an enhanced understanding of evacuation routes and potential challenges during flood events, ultimately contributing to more efficient emergency preparedness and response. Additionally, human insight takes on a new dimension through integrating X data, which acts as a conduit for real-time, on-the-ground observations during flooding. Leveraging the X Application Programming Interface (API), this data stream offers a unique window into localized experiences and concerns, bridging the gap between data-driven forecasts and the human dimension of disaster response. By incorporating these human-generated insights into the flood evacuation prediction pipeline, a holistic view emerges, enriching the decision-making process and empowering authorities with nuanced perspectives on at-risk locations and specific scenarios. In this integrated framework, the fusion of gauge height predictions, a river hydraulic model, transportation data, and real-time X observations heralds a transformative paradigm in flood evacuation prediction and response strategies.

Several studies have led to increased growth in HAC literature, where humans and AI data meet at a point to work together in collaboration and carry out complex tasks as an integrated unit. However, HAC has never been applied for flood emergency decision-making and response, and perhaps this area needs special attention and creative solutions.

Indeed, analysis of HAC for flood evacuation emergency management requires humans and AI corporations to form the basis for its applications and developments in real time. This thesis examines the benefits of employing a HAC in flood evacuation planning and the decision-making process; no intention is to include all possible works, applications, or techniques, but rather to provide a big picture of some paths for future research.

In this study, we addressed the current gaps and challenges and how the HAC paradigm can help to improve flood evacuation decisions. This study discusses that lack of teaming intelligence is one of the most prominent gaps in flood disaster management. Understanding how AI can be used as a teammate in real-time and highly collaborative scenarios is crucial to shedding light on how the HAC paradigm should be structured to suggest evacuation re-routing and improve flood emergency decision-making from a human perspective.

This study aims to establish a comprehensive methodology for gauge height and river hydraulic prediction through the synergistic utilization of machine learning models and social media data. The process involved developing and training a machine learning model to forecast river gauge height, a pivotal factor in visualizing potential flood extents. This predictive model will be foundational for flood modeling, generating precise depictions of inundation areas on a geographical map. To enhance predictive accuracy and encompass the human dimension, incorporating human-generated data is planned by leveraging the X API to extract flood-related X posts (formally known as Tweet) from

South Carolina and mapping the X post's geolocations. The map interface is an intermediary, facilitating seamless interaction between human-contributed data and machine learning-generated predictions. A pioneering study aspires to be delivered through this approach that advances flood evacuation prediction and disaster management methodologies.

CHAPTER TWO

RESEARCH QUESTIONS

Developing an effective flood evacuation prototype necessitates a comprehensive exploration of critical research questions, encompassing a multidimensional perspective to enhance flood prediction, response, and decision-making. Addressing these questions is pivotal to fostering a holistic approach to disaster management. Developing a flood evacuation prototype will involve addressing the following research questions:

1. How can we programmatically identify potential roads at risk of flooding over large coastal drainage networks based on observational sources such as river stage gauges, crowdsourced data (e.g., X data), and transportation network information?
2. How can human and AI collaboration be leveraged to improve flood prediction and enable more informed evacuation decisions?

CHAPTER THREE

LITERATURE REVIEW

3.1 Human-AI Convergence Studies

The seeds of AI were in the mid-20th century with the question **"Can machines think?"** which considered if machines could mimic human intelligence [9]. This question laid the foundation for machine intelligence and AI system development. As research progressed and AI grew, researchers started addressing **"How can machines think and work for humans."** To address this question, numerous algorithms such as Long Short-Term Memory (LSTM) [10], Convolutional Neural Networks (CNN) [11] and Support Vector Machine (SVM) [12]. As AI research has progressed, machines have largely supplanted humans in real-world contexts such as healthcare, transportation, finance, military, and disaster support applications. Today, the world views AI as a tool. However, this focus is shifting toward viewing machines as a collaborative partner rather than a tool.

Achieving the successful development of an AI system that can function as a good teammate will require advances in the design and measurements. Proper modeling practice is crucial in designing, developing, and testing the new HAC systems, particularly concerning system development based on real-time decisions. However, achieving this goal of creating proper HAC requires that the AI systems be highly reliable and robust within the range of flood evacuation conditions in which they might be employed and that

these systems operate seamlessly within a much larger and more complex set of data and human observations.

The study of human-only teams led to the foundation of human AI teaming. The study of who, what and how the human could team began in the 1980s [13]. This study examined the human team dynamics and iterated how this team could perform better. Another study [14] created a Team Evolution and Maturation (TEAM) model, which posits that teams can develop in various ways. The author also conducted an experimental investigation on this model, and the findings informed us that teams can be developed in multiple ways and rates. Each team is believed to be unique in its way. [15] focuses on a military team and highlights the military's role in military team cohesion, loyalty, and performance. Using military team as an example, this research discussed broader implications on various types of teams in different organizations.

From a human perspective, teaming has moved into HAC. This move wasn't straightforward, and it started with works of literature presenting the theoretical foundation to HAC. In a review of teaming studies, [16] found various roles for humans and AI to tackle the position of explorer, investigator, teacher, and Judge, where AI should take a role in calculating and identifying relevant information. [17] proposed a framework in the educational sector to enhance collaboration between humans and AI. This research illustrates that humans guide, design, and train AI to take on more tasks slowly as they evolve. Another study [18] also presented a conceptual framework of how humans and AI

could work together. This research suggested that a unique Educational AI (AIEd) system and human facilitators might augment one another.

Another study [19], described human–machine collaboration on various economic scales (microscale, mesoscale and macroscale) to boost financial and environmental sustainability. This study suggested that merging AI with help automation in the artisanal economy would require supportive policies, metrics and changes in infrastructure. Another study, [20] presented a synergistic future for human and AI collaboration in media and communication. This study emphasized how humans and AI work together in previous studies. This paper suggested that AI helps humans in decision-making and extending human capabilities while humans work to direct and refine AI. This paper underscored the importance of creating interfaces where humans and AI can interact.

Previous research exploring how humans and AI can work together suggests various roles and responsibilities for humans and AI collaboration frameworks. Each study suggests a common thread that humans and AI hold promise for the future. These researchers also recommended that in human-AI collaboration, humans and AI should assume roles in which they specialize. AI should take roles like calculation/computation and learning from extensive data, whereas humans should take roles in guiding and training by embracing creativity.

These studies have built the theoretical foundation of human-AI collaboration. Other studies have used game simulation to assess the impact of collaboration between humans and AI systems, which would converge the knowledge of humans and AI in a team. For example, [21] used a gaming platform named Rocket League to study how varying levels of AI teammates impact human performance. Authors found that humans perform better when the influence of AI gradually decreases using the gaming platform. The researcher also indicated that people do not judge AI by how it performs but if only it aligns with the goal of humans. Finally, the researchers concluded by suggesting that it is more important to prioritize human learning and growth in HAC. Another study [22] used the computer game Minecraft to access human agents and urban search and resume autonomous agent collaboration. The outcome of this study shows that the collaboration between AI and humans is degraded when there is limited communication. Also, a higher workload was felt when the participants were not informed of external challenges. This research concluded that a human-AI team must have effective communication, mutual understanding, shared beliefs, and knowledge to perform well. In another effort, [23] used a chess game to explore the effects of human perception when working with an AI teammate. Their finding revealed that while an expert player focuses on AI performance improvement, the less skilled player can have more influence on AI teaming. This research also highlights that deceiving human about their AI teammates can degrade trust and performance. It is also essential to consider individual expertise when teaming with AI.

Past studies show that game simulation has become very helpful in mimicking the real-world scenario. This controlled environment has helped to test the hypothesis of human-AI collaboration in a near real-world environment without any risk. The findings from these studies underscore that, like all human teams, it is essential to have effective communication, mutual understanding, shared goals, and trust in a human-AI collaboration. These game simulations also revealed that performance and efficiency have increased when AI collaborates as a teammate with a human. The findings from the game simulation were helpful for a test scenario, but to move forward in the realm of AI, we should test human-AI collaboration in a real-world scenario.

Nonetheless, a few pioneering studies have ventured beyond the theoretical realm to explore practical implementations of converging the knowledge of humans and AI. One research [24] that worked beyond the theoretical area is Watch-And-Help (WAH), a challenge for testing social intelligence in AI in everyday household activities. In this research, an AI agent collaborates with a human-like agent in two stages to achieve the goal function faster. The first is the Watch stage, where an AI agent watches a human-like agent performing a task once and infers a human-like agent's goal from her actions. The second stage is the help stage, where an AI agent helps a human-like agent to achieve the same goal in a different environment as quickly as possible. The results show that the AI agent can complete the WAH challenge, but it is less effective than human participants. The authors concluded that the WAH challenge is valuable for evaluating AI agents' social perception and human-AI collaboration capabilities. They suggested that future research

should focus on developing AI agents to perform the WAH challenge more effectively than human participants. Another research [25] goes beyond the theoretical area and identifies the relationship between anticipatory information pushing and trust in human–autonomy teaming in a remotely piloted aircraft (RPA) system. This study finds that in deteriorating circumstances, trust in AI teammates decreased while trust in human teammates increased. Also, anticipatory information increases confidence among human colleagues but not AI colleagues.

Previous studies have demonstrated that AI advances to surpass humans as competent partners. More research is needed to understand human and AI collaboration and knowledge sharing in a real-world scenario. Past studies used some form of hardware (for example, a robot) to support the HAC framework. However, these are not cost-effective, and deploying this system in a large geographical region for a real-world scenario will be challenging. This is the reason why a HAC system does not yet exist in the disaster evacuation domain. If we eliminate the hardware dependency, the system can be cost-effective as implementation across vast geographical areas in real-world settings becomes more manageable. This opens a gateway for HAC applications in disaster response and decision-making problems. To create a flood disaster evacuation tool, we should train the machine learning model and then couple it with a river hydraulic model along with leveraging real-time human knowledge and geospatial information, which can improve the performance of evacuation decisions. Adding much human knowledge to a system in real time can increase trust in HAC implementations. In addition, incorporating additional

human data through social media is deemed to be useful for improving disaster decision-making [26].

3.2 Data-driven Flood Forecasting Studies

Flood forecasting research is evolving from traditional methods to more intelligent, data-driven approaches. Flood modeling helps understand the past and current state of the rainfall-runoff mechanism in a watershed and provides a way to explore the implications of management and planning decisions. Several modeling efforts have been conducted in complex watersheds, such as coastal drainage systems based on lumped and physically based simulations [27] [28]. [27] studied a Power-Law Regression Model (PLR) and [28] focused on fuzzing techniques. [29] employed a physics-based flood model and coupled the flood system with Bayesian uncertainty models. They suggested that large uncertainty, particularly during runoff peak rates simulation, can dimmish flood prediction accuracy and performance.

However, the rapid increase in the availability of measurement data has spurred the development of many data-driven methods or ML approaches for modeling and predicting flood dynamics [30]. Machine learning algorithms attempt to estimate the mapping function (f) from the input variables (x) to numerical or continuous output variables (y) and can learn the patterns hidden in data. Several studies have demonstrated the use of machine learning in flood modeling. For example, [31] [31] [32] built feedforward networks and

proposed a neural network model that did not require many dataset pieces. [33], [34] considered the application of support vector machines (SVM) for flood forecasting. These authors proposed an SVM-based solution for flood forecasting problems but also discussed that SVM was prone to overfitting and underfitting and needed to perform various trial and error tests before reaching an optimal result.

More recently, neural networks such as RNNs have been used to predict rivers' sequential values and water height [35]. Previous research (examples [36] and [35]) used LSTM to forecast the river's hydrological conditions. These studies presented a great approach to predicting the river's hydrological situation during historical periods. However, citizens would need real-time information, including flood height and inundation extent, during real-time flooding events to make intelligent decisions in advance. [37] underscored the use of LSTM in Google's operational flood forecasting system (operational since 2018), which has helped save lives and reduce damages in regions in India and Bangladesh prone to flooding.

Traditionally, tools like flood warning systems, Geographic Information Systems (GIS), and transportation infrastructure plans are used for flood evacuation decisions in South Carolina. Flood warning systems use real-time data from sensors and weather forecasts to predict flood risks and issue alerts to residents in affected areas. For example, the National Weather Service (NWS) provides a nationwide network of flood warning systems that issue alerts via text message, email, or social media. The public only receives

this warning through text messages, emails, or social media feeds. However, some residents need smartphones to access the notifications and alerts, and those who access the alert information need help understanding and navigating the data. GIS tools can map flood risks, identify evacuation routes, and plan evacuation strategies. South Carolina Emergency Management Division (SCEMD) uses GIS tools and transportation infrastructure plans to map vulnerable locations and paths to help emergency managers plan evacuation decisions. However, these GIS tools can only be used with technical knowledge. Also, the South Carolina Department of Transportation (SCDOT) has developed evacuation routes and zones to identify safe roads to help residents evacuate quickly and safely during a flood event.

Flood evacuation can be a difficult and stressful experience for those involved. Evacuation decisions often tend to be sudden or unexpected. Although a few tools, such as [38] [39] [40] are available for flood evacuation, these tools are not accessible or are not simple to use and understand by citizens. Furthermore, these tools do not coordinate with humans to validate evacuation decisions and responses.

CHAPTER FOUR

STUDY AREA

HAC approaches were developed and tested for the Lowcountry in South Carolina, where frequent flooding caused significant damage to people's lives, properties and critical infrastructure. A flat terrain and low elevation, prone to inundation conditions during heavy rainfall and storm surges, characterize the Lowcountry. Given the region's increased vulnerability to flooding, substandard roads in rural areas and relatively larger population density, the developed HAC approach was tested and validated for the Lowcountry of South Carolina. Previous instances of flooding and hurricanes in the region, such as the South Carolina Flood in 2015 and Hurricane Matthew in 2016, resulted in significant fatalities and damage. Thus, the primary objective of this research study is to understand flood evacuation decisions and model evacuation routes during flood emergency conditions.

We considered various gauging stations in Lowcountry, South Carolina, as case studies for this research (see Figure 4.1). River's data was collected from the United States Geological Survey (USGS) and NWS. We trained the machine learning models for five USGS gauging stations located in the Lowcountry, explained below.

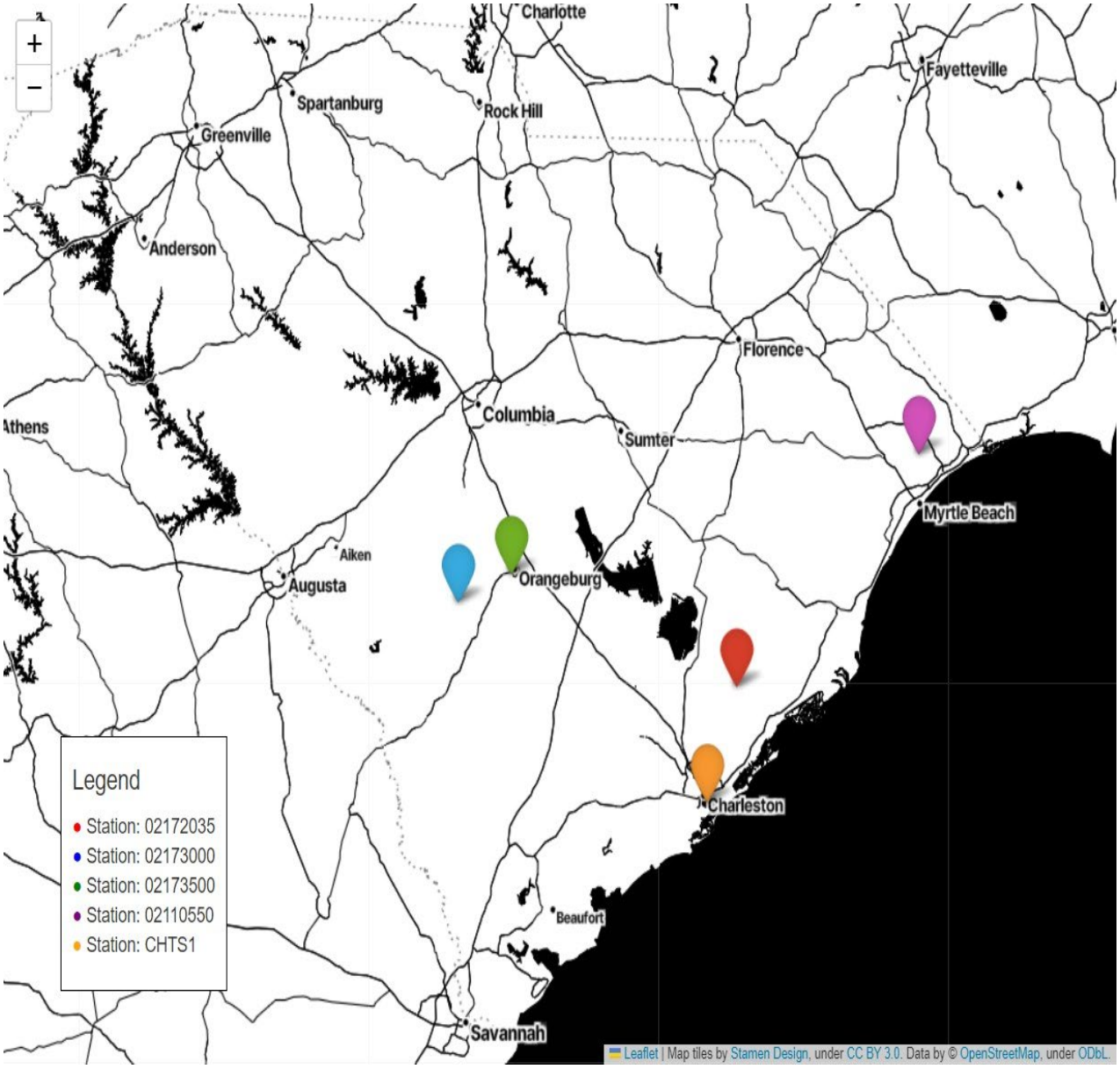

Figure 4.1: The USGS gauging stations used in this research.

4.1 Case Study 1: Turkey Creek River

Turkey Creek gauging station (USGS02172035) is located above Huger, South Carolina. Current and past discharge, gauge height, and precipitation conditions have been

available since 2005. The river gauge height data is available every 15 minutes. The drainage area for this gauging station is 19.8 square miles. The South Atlantic WSC Charleston Field Office manages this station.

4.2 Case Study 2: South Fork Edisto River

South Fork Edisto River gauging station (USGS02173000) is located near Denmark, South Carolina. Several hydrologic data, such as river discharge, gauge height, and precipitation conditions, are available at this site. Discharge data has been available since 1930, gauge height data since 2007 and precipitation data since 2015. The data on this river is also available every 15 minutes. The drainage area for this site is 720 square miles. The South Atlantic WSC Columbia Field Office manages this station.

4.3 Case Study 3: North Fork Edisto River

North Fork Edisto River gauging station (USGS02173500) is located in Orangeburg, South Carolina. Current and past discharge, gauge height, and precipitation conditions are available for this site. Discharge data has been available since 1986, gauge height data since 2007, and precipitation data since 2014. The data on this river is also available every 15 minutes. The drainage area for this site is 683 square miles. The South Atlantic WSC Columbia Field Office manages this station.

4.4 Case Study 4: Waccamaw River

Waccamaw River gauging station (USGS02110550) is located above Conway, South Carolina. Current and past discharge, gauge height, and precipitation conditions have been available at this site since 2013. The data on this river is also available every 15 minutes. The drainage area for this site is 1,250 square miles. The South Atlantic WSC Columbia Field Office manages this station.

4.5 Case Study 5: Cooper River

Cooper River gauging station is located in Charleston Harbor. NWS Advanced Hydrologic Prediction Service (AHPS) issues every-hour forecasts for this site, which are published routinely year-round. This forecast can be parsed and used out of the box without creating a ML model. This site is also located in Charleston and is considered a crucial site for flood forecasting in the Charleston area.

.

CHAPTER FIVE

METHODOLOGY

5.1 Human Data

Human input is a crucial component of HAC architecture. Human data collection is usually chaotic. However, with the rise in technology, gathering human data has become less complicated. Several methods for collecting human data exist, such as (i) interviews/focus group discussions and(ii) social media, search engines, and web scraping. This research collects human data using interviews and social media (X).

5.1.1 Human Data from Interviews

We have conducted several interviews and focus group discussions with various stakeholders, including SCEMD, SCDOT, and the South Carolina Department of Public Safety (SCDPS), to acquire their attitudes and perspectives on flood evacuation decisions. In these interviews, we learned about the history of flood evacuation decisions, tools, current obstacles, and ideas for improvement. Unfortunately, none of the organizations with which we've conducted interviews maintain a flood evacuation tool; instead, they rely on data from external sources such as USGS and NWS and transportation infrastructure planning. USGS and NWS contain information such as the river's current and future forecasts. However, converting the numerical data from USGS and NWS into standard format presents a substantial barrier for organizations engaged in the Lowcountry flood evacuation decision. These numerical statistics provide river conditions, but they face a

tremendous issue in determining the extent of a flood in a particular region. To address this issue, we used the HAND method and a visualization approach to map flood inundation areas.

5.1.2 Human Data from X API

Machine learning models are an excellent tool to predict flooding events. However, these tools alone may not capture all the pertinent information required for accurate flood prediction. In addition, flood data is highly variable, making it difficult to construct proper models. In addition, the quality and precision of the data used to train machine learning models can limit their reliability. Although machine learning models can help predict flood events, they should be supplemented with other methods to ensure accuracy. By providing real-time updates, diverse perspectives, and contextual information that machine learning models alone may not be able to capture, adding human knowledge, such as data obtained from social media platforms such as X, can improve machine learning's capacity to predict flood events.

The X API is a valuable tool for collecting X posts related to flooding because it provides real-time updates on flood conditions and evacuation efforts. The X API enables developers to search for messages using particular keywords or hashtags, making it simple to collect relevant data. The keywords that were used to search for X posts in this project include “floods,” “flood emergency,” “road damage,” and "evacuation". These keywords can be customized by the user to collect data on specific flood events or locations. In this

study, only X posts from South Carolina are retrieved. The X API also provides metadata about messages, such as location and time, which can be used to filter and analyze the collected data. In addition, we have designed a text classification model to filter only those X posts that are relevant to flooding.

5.1.2.1 X post Classification

This study used Google's Bidirectional Encoder Representations from Transformers (BERT) package to classify X posts. BERT is a cutting-edge, pre-trained Natural Language Processing (NLP) model with sophisticated neural network architecture and capacity for contextual text analysis [41]. The BERT model can generate high-quality representations of natural language text by simultaneously considering the entire input sequence of words to the left and right of the target word, thereby enabling more contextually relevant representations. In contrast to previous NLP models, which only considered the context of the target term's left and right, this model considers the entire sentence.

To classify an X posts related to flooding using BERT, the model can be trained on a labeled dataset of X posts, where each X post is categorized as relevant or irrelevant to flooding. We first created a text classifier on top of the BERT model. We then collected the dataset from various sources [42] [43] [44] [45] [46] [47] to train BERT. These data sources also contain irrelevant X posts so that BERT could learn the distinction between relevant and irrelevant X posts by accumulating irrelevant X posts alongside relevant ones

during training. By including irrelevant X posts in the training data, the model learned to differentiate between various categories of X posts and identified which specific features or keywords indicate whether a X post is relevant or irrelevant to flooding. Each text was then given a category of 0 (not relevant) or 1 (relevant). During the process of fine-tuning, the BERT model learned to identify key flood-related textual features and used them to make accurate predictions.

The fine-tuning process involved training the BERT model on the labeled dataset and adjusting its parameters to classify relevant X posts. A backpropagation method was used for the text fine-tuning process. The model was trained for 30 epochs. The model's predictions were compared to the true labels, and the model's parameters were adjusted to minimize the difference between the predictions and the true labels. Once the BERT model was fine-tuned, it was used to classify new, unlabeled X posts as either relevant or irrelevant to flooding. The text of the X post is input into the BERT model to classify a new X post. The model's output is a probability score indicating the likelihood that the X post is relevant to flooding. If the probability score is above a threshold of 80%, the X post is classified as relevant to flooding. After the X posts were collected using X API in real-time, we performed text classification of collected X posts. This text classification decided whether the X post was relevant to a flood disaster or not.

5.1.2.2 Performance Metrics Used in X post Classifier

To evaluate the performance of the BERT model for classifying flooding X posts, we used three standard performance metrics: accuracy, precision, and recall. Accuracy measures the model's overall performance and represents the percentage of X posts correctly classified as relevant or irrelevant to flooding. This metric is essential for evaluating the general effectiveness of the model. Precision measures the proportion of correctly classified relevant X posts among all X posts classified as relevant by the model. This metric is essential for evaluating the accuracy of the positive predictions made by the model. Recall measures the proportion of correctly classified relevant X posts among all relevant X posts in the dataset. This metric is essential for evaluating the completeness of the positive predictions made by the model. Equations 1, 2, and 3 are accuracy, precision, and recall formulas, respectively. In these equations, *TP* denotes true positive, *TN* is true negative, *FP* represents false positive, *P* is total positive classes, and *N* denotes total negative classes.

$$\text{Accuracy} = \frac{\text{TP} + \text{TN}}{\text{P+N}} \quad \text{(Equation 1)}$$

$$\text{Precision} = \frac{\text{TP}}{\text{TP} + \text{FP}} \quad \text{(Equation 2)}$$

$$\text{Recall} = \frac{\text{TP}}{\text{TP} + \text{FN}} \quad \text{(Equation 3)}$$

5.2 Gauge Height Forecast

Gauge height, also known as flood stage, is the height of the water surface above a specified reference point, such as a fixed point on the riverbank or the riverbed. It is typically measured using a water level instrument or stream gauge instrument installed at a specific location along the river. Gauge height is an important parameter for monitoring and predicting flooding, as it can estimate the volume of water flowing in the river.

We used machine learning algorithms, NWS AHPS forecast data, and a Rational method along with a rating curve conversion tool to predict flood level (or gauge height of the river) in ungauged/poorly gauged watersheds in the Lowcountry. USGS has developed a comprehensive database system, freely available online, that enables users to access a diverse array of water-related data and information to train machine learning algorithms. USGS National Water Information System (USGS NWIS) is a comprehensive repository of data pertaining to water resources, encompassing details on the physical, chemical, and biological properties of rivers and watersheds. This information is gathered via a comprehensive network of nationwide monitoring stations. These stations are responsible for the measurement and recording of diverse hydrological parameters.

Historical time series data of precipitation and discharge obtained from USGS NWIS were used to train machine learning algorithms. Precipitation and discharge are two important variables that were incorporated into machine learning models to predict gauge height values. The depth of a river, and hence the gauge's height, is directly determined by

its discharge, which quantifies how much water flows through it in a fraction of time. The river's depth typically rises as the flow increases, boosting the gauge's height. On the other hand, rivers can receive water from river basins through precipitation. Rainfall has an impact on river flows both directly and indirectly through several hydrological procedures, such as surface runoff mechanisms and groundwater recharge. Increased precipitation may cause more significant river flows, affecting gauge height. As a result, by monitoring and analyzing flow and precipitation data, we can train machine learning algorithms and use the pre-trained models to forecast floods.

It is important to note that the gauge height of the river was a slow-changing parameter during no-flood events, while its values changed significantly during flooding events over short intervals of 15 minutes. Since the flood prediction task was based on an hourly basis, we used an aggregation engine that calculated the cumulative number of bytes (15 minutes) on a daily basis. Since several watersheds in the study area were poorly gauged, we used the NWS AHPS River forecast. If NWS AHPS was not available, we then calculated flood level using a Rational model.

5.2.1 Machine Learning Algorithms

We trained two types of RNN models, i.e., LSTM and Gated Recurrent Unit (GRU), [48] for four USGS gauging stations. For each station, we used Optuna [49] to optimize the best hyperparameters. We trained 30 models for each station (240 models [2 models, 4 stations and 30 models each]) and used the best model for flood forecasting.

During training, we used the pruning technique in Optuna as an early stopping technique. Pruning within the Optuna hyperparameter optimization library stops RNN training early if it is deemed unlikely to produce a better result than the previous best-known model configuration. Using the pruning technique, we can stop the model training intelligently and efficiently if it is deemed unlikely to produce better results without sacrificing the quality of results. From 240 models produced during training, eight best models were selected from the Optuna library (for four gauging stations and two models), and then four best models were chosen manually by looking at the performance metrics.

We applied LSTM and GRU to forecast gauge height. The architecture of an RNN variant has been specifically developed to address the issue of vanishing gradients that are commonly encountered in conventional RNNs. LSTM networks are equipped with a specialized memory cell that is capable of retaining information for extended periods. Additionally, these networks feature three distinct types of gates - namely, the input gate, forget gate, and output gate - which regulate the inflow and outflow of information to and from the memory cell. The gates incorporated in the network facilitate the selective retention or omission of information, rendering it highly appropriate for applications that entail the manipulation and retention of sequential data, such as NLP, speech recognition, and time series prediction. The LSTM network receives input data as a sequential vector set, with each individual LSTM unit processing a single vector at each time step. The output of each LSTM unit is a hidden state vector that is subsequently utilized as input for the following time step. The LSTM model can effectively model intricate sequential data by

using gates to regulate the flow of information within the network. This enables the model to retain information from past inputs and leverage it to make informed predictions about future inputs. As a result, LSTM is a highly potent tool for modeling complex sequential data like flood data.

Our study employed a neural network architecture consisting of six LSTM layers dropout and a dense layer. The first three hidden layers were followed by a dropout layer, and then the dropout layer was followed by the remaining LSTM layers. This was followed by a flattened layer and a dense layer containing five neurons. The spatial dimensions of the input are reduced to the size of the channel by a flattened layer. The LSTM layer is designed to predict the subsequent 5 data points (5 hours) by utilizing the preceding 48 data points (48 hours). The dropout rate, number of units for each layer and epoch number were decided after training 240 models using Optuna. This is because the quantity of water flowing into and out of a river system affects the height of a gauge. The river system receives runoff from precipitation, whereas the runoff output from the system is represented by discharge. The primary source of water in rivers is precipitation, which exhibits significant spatial and temporal variability. In hydrological forecasting, incorporating precipitation data is crucial for accurate gauge height prediction as it enables the capture of temporal fluctuations in flood data patterns. The discharge, which pertains to the quantity of water passing through a river's cross-sectional area per unit of time, is a crucial variable to take into account as it indicates the volume of water present within the river system. The discharge of water can be influenced by a range of factors, including but

not limited to precipitation, snowmelt, groundwater discharge, and anthropogenic activities such as dam operations and water withdrawals.

5.2.2 Performance Metrics

Several significant performance measures are utilized to assess the RNN model's performance. They are Mean Square Error (MSE), Mean Absolute Error (MAE), Mean absolute scaled error (MASE), the Nash–Sutcliffe model efficiency coefficient (NSE), and Huber Loss.

MSE (Equation 4) is the average square of the difference between the model's predicted data and the actual data throughout the whole dataset.

$$MSE = \frac{1}{n}\sum_{i=1}^{n}\left(Y_i - \hat{Y}_i\right)^2 \quad \text{Equation (4)}$$

Where:

- $\hat{Y}_i$ is predicted data.
- Y_i is actual data.
- n is the length of dataset.

MAE (Equation 5) is the average magnitude of the difference between the model's predicted data and its actual data for a collection of predictions and observations as a measure of the magnitude of errors for the entire dataset.

$$MAE = \frac{\sum_{i=1}^{n}|Y_i - \hat{Y}_i|}{n} \quad \text{Equation (5)}$$

Where:

- $\hat{Y}_i$ is predicted data.
- Y_i denotes actual data.
- n represents the length of the dataset.

MASE (Equation 6) is an alternative to metrics like MAE to provide a more interpretable scale. To calculate MASE, we divide the MAE of the forecasting method with the MAE obtained when using the previous observation as the forecast for the next observation.

$$\text{MASE} = \frac{\text{MAE}_{\text{forecast}}}{\text{MAE}_{\text{naive}}} \qquad \text{Equation (6)}$$

Where:

- $\text{MAE}_{\text{forecast}}$ is Mean Absolute Error of the forecast method.
- $\text{MAE}_{\text{naive}}$ represents Mean Absolute Error obtained when using the previous observation as the forecast for the next observation.

The NSE (Equation 7) is used to evaluate the hydrological models' forecasting ability. NSE indicates how well the plot of actual and predicted data fits a 1:1 line.

$$\text{NSE} = 1 - \frac{\sum_{i=1}^{n}(Y_i - \hat{Y}_i)^2}{\sum_{i=1}^{n}\left(Y_i - Y_i^{mean}\right)^2} \qquad \text{Equation (1)}$$

Where:

- Y_i is observed data at time step i.
- $\hat{Y}_i$ represents the predicted or modeled data at time step i.
- Y_i^{mean} mean of the observed data.
- n denotes the total number of observations.

The Huber loss (Equation 8) is a robust loss function used in regression problems. It combines the properties of the MAE and the MSE. The Huber loss is quadratic for small error values (similar to MSE) and linear for large error values (similar to MAE), making it less sensitive to outliers than the MSE.

$$L_\delta\big(y, f(x)\big) = \begin{cases} \frac{1}{2}\left(y - f(x)\right)^2 & if\ y - f(x)\ \leq\ \delta \\ \delta \mid y - f(x) \mid - \frac{1}{2}\delta^2 & otherwise \end{cases} \quad \text{Equation (8)}$$

Where:

- y is the true value.
- $f(x)$ denotes the predicted value.
- δ represents a threshold value.

5.2.3 Rational Method

The Rational method (Equation 9) is a deterministic hydrological tool commonly used for estimating an ungauged watershed or catchment 's peak flow rate or discharge. It

is based on the principle that the peak flow rate is directly proportional to the rainfall intensity, the area of the catchment, and a runoff coefficient that considers the characteristics of the land use and soil type in the area. This method uses a simple mathematical equation to estimate flood peak discharge (Q) based on three inputs: the rainfall intensity (I), the drainage area (A), and the runoff coefficient (C). The equation is given as:

$$Q = \frac{C*I*A}{360} \quad \text{Equation (9)}$$

The Equation 9 involves:

- The measurement of I in inches per hour (in/hr).
- The expression of A in acres.
- The utilization of C as a dimensionless factor.

To obtain the value of Q in cubic feet per second (cfs), it is necessary to divide the product of C, I, and A by 360. The product of the values of C, I, and A is first divided by 12 to convert the unit of measurement from inches to feet and subsequently divided by 60 to convert the unit of measurement from hours to minutes. This calculation yields a factor of 1/720. This value is subsequently multiplied by 3600, which serves to convert minutes to seconds, resulting in a factor of 1/360. The computation of Q in cfs is obtained through division by 360. The Rational method is employed in cases where there is insufficient data to facilitate flood prediction and when the NWS AHPS fails to furnish a river forecast.

The initial step in computing the runoff coefficient involves obtaining the land use data for a specific latitude and longitude through the utilization of the overpass API. A coefficient is assigned to each type of land use. The OpenWeatherMap API is utilized to obtain data on rainfall intensity. The drainage area can be obtained by utilizing a digital elevation model (DEM) specific to the low-country region of South Carolina. Initially, the metadata of DEM was extracted, encompassing details such as the pixel dimensions and transformation data. Subsequently, the provided latitude and longitude values were transformed into pixel coordinates utilizing the available transformation data. A threshold value was subsequently employed on the DEM to generate a binary mask that denotes the watershed region. Finally, the computation of the watershed's drainage area involves the summation of the mask, which is then multiplied by the pixel area. The calculated drainage area is expressed in units of square meters and converted to acres through division by 4047. By utilizing these three variables, it is possible to derive the maximum discharge of water in a river.

A rating curve approach was then employed to convert the maximum discharge obtained from the Rational method's equation into gauge height. The rating curve was established by the USGS as an empirical correlation known as a "rating curve" linking the stage of a river to its stream discharge. The rating curve represents the correlation between the height of a measuring instrument and the volume of water flowing in a stream. In order to generate this curve, the USGS conducts site visits to all gauges on a biweekly basis and obtains stage and river discharge measurements through manual means.

5.3 HAND Model

We formulated the HAND model as an [50] inundation mapping approach in Python to depict the potential extent of flooding. The HAND model is a terrain analysis technique that estimates the elevation of a point above the nearest stream or river. The model is extensively employed for the purpose of ascertaining the flood risk, drainage patterns, and erosion potential of a given region. The HAND model is founded on the principle of surface elevation and the idea that water moves in a downward direction from elevated to lower altitudes, ultimately accumulating water in low-gradient areas with a potential for ponding conditions. Consequently, the vertical distance between a given point and the closest stream or river is crucial in determining the likelihood of water movement toward the downstream portion. The initial step in generating a HAND model involves utilizing a DEM model to produce a flow accumulation map. The map portrays the number of cells that contribute to the flow of each cell within the digital elevation model. Typically, the cells exhibiting the greatest flow accumulation are situated in proximity to the streams and rivers. Subsequently, a distance transform algorithm determines the distance between each cell in the DEM and the closest stream or river. Subtracting the elevation of individual cells in the DEM from the distance to the closest stream or river results in the computation of the HAND value for that particular cell. The utilization of HAND values is viable in the creation of a HAND map, which effectively displays the altitude of individual points in relation to the nearest stream or river. The HAND map has the potential to facilitate the

identification of regions that are susceptible to flooding, areas with inadequate drainage, and locations that are prone to surface ponding conditions.

The HAND model utilizes a pair of methodologies on a DEM to normalize the terrain in relation to the hydrological network. The initial stage involves executing a sequence of computations to produce a DEM that adheres to hydrological principles, establishes pathways for water flow, and allocates drainage channels. The subsequent phase entails employing indigenous drain orientations and the drainage system to generate the nearest drainage chart, which will subsequently guide the HAND operator in establishing the normalized topology of the HAND model in a spatial manner. The HAND model is classified into various classes based on the severity of the inundation. These classes include class 1 (0 to 0.5 meters), class 2 (0.51 to 1 meters), class 3 (1.1 to 1.5 meters), class 4 (1.51 to 2.0 meters), class 5 (greater than 2.0 meters). The HAND model postulates that inundation occurs when the elevation of water surpasses the altitude above the adjacent stream or drainage. The HAND methodology involves assigning a value to each pixel in a raster, which represents the relative elevation in meters between the pixel and the nearest water stream. Equation 8 provides the map algebra equation for calculating inundation that is equal to or less than the HAND value.

$$\text{HAND raster} < x \qquad \text{Equation (8)}$$

where, x is the height of water.

Figure 5.5 presents a step-by-step example of HAND calculation. For the last step (i.e., step 8), Equation 8 is used to calculate the inundation and integer 2 is considered the flood depth.

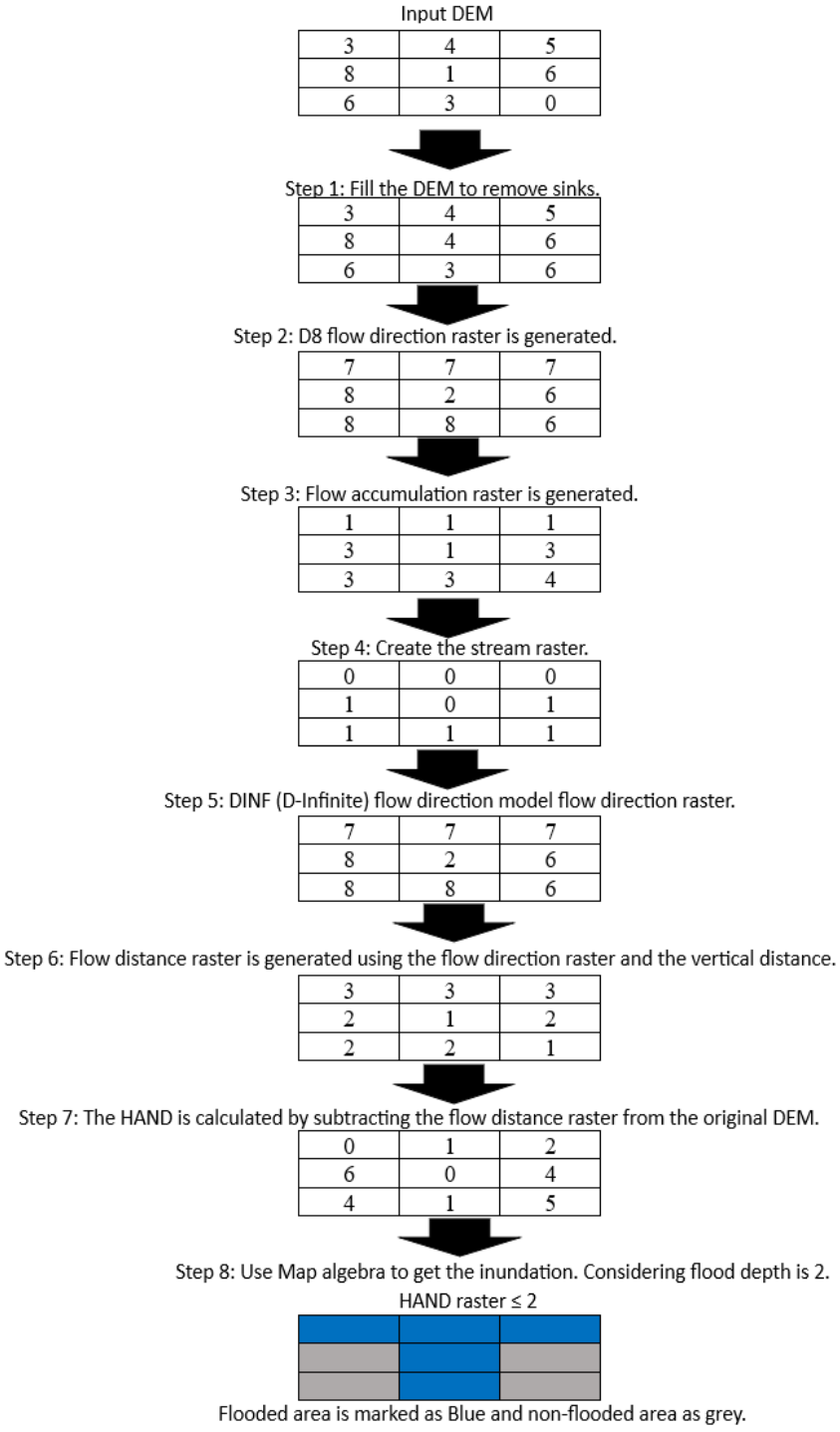

Figure 5.1. The workflow of HAND calculation.

We transferred the HAND inundation approach along with RNN models to a web application to visualize flood inundation and suggest evacuation re-routing. Initially, the HAND elevation data was acquired from [51] and generated a hydrological terrain raster, known as HAND, for a Hydrologic Unit Code 6 (HUC6) region in the contiguous United States (CONUS). This was achieved by utilizing a DEM with a 10-meter resolution obtained from the USGS 3-D Elevation Program (3DEP) and the National Hydrography Dataset (NHD) Plus hydrography dataset. The HAND data was then generated by utilizing data sources such as stream networks. Then, the aforementioned data was amalgamated with the hydraulic property data to generate an all-encompassing dataset. Subsequently, the map algebra approach in Python was used to compute the HAND value for each raster grid.

Next, the HAND map was categorized into several classes. These classifications represent varying depths of flooding, ranging from deep to shallow water. This categorized HAND raster was finally put in a web application utilizing a JavaScript library leaflet.

5.4 Transportation Networks

We have combined the HAND model with transportation geospatial data, including highways, trains, evacuation zones, and evacuation routes. We included data on highways and railroads from the TIGER (Topologically Integrated Geographic Encoding and Referencing) database. Additionally, we added SCDOT evacuation routes and SC

Hurricane Evacuation Zones. The United States Census Bureau initially created the TIGER database to assist the decennial census, which is carried out once every ten years. In-depth geographic data on the United States, such as the locations and features of roads and railroads, can be found in the TIGER database. Each year, emergency management officials designate some geographic locations in South Carolina as hurricane evacuation zones because they are vulnerable to storm surges and other hurricane-related risks. These areas have been set aside to assist locals and tourists in South Carolina determine whether they should stay in a location that storm surges might impact and whether they should evacuate before a hurricane. The Hurricane Evacuation Zone maps are updated and maintained by the SCEMD to guarantee the information's accuracy and the efficacy of the evacuation strategy. The SCDOT has authorized several evacuation routes for usage in an emergency. These routes are designed to ensure the safety of locals and visitors during storms, flooding, or other natural catastrophes. These roads are intended to divert traffic inland and away from the shore to safer regions.

The integration of various transportation networks has been achieved through ArcGIS REST (Representational State Transfer) API services and the Esri Leaflet plugin. Esri provides ArcGIS REST, web-based services that enable users to access, visualize, and analyze geospatial data. The services are founded on the RESTful design pattern and rely on HTTP requests and responses for intercommunication between the client and server. Esri Leaflet plugin is an open-source Leaflet plugin. This provides an easy way to integrate ArcGIS REST services and ArcGIS Server map services into Leaflet-based web mapping

applications. The plugin encompasses a collection of classes and functions that facilitate the integration of ESRI layers, such as feature layers, dynamic map layers, and tiled map layers, into Leaflet maps for developers. The ESRI layers were integrated with the OpenStreetMap layer to generate interactive maps for end-users.

5.5 Evacuation Re-routing

Evacuation planning is critical to disaster management, as it involves identifying safe routes for evacuees to follow. Recently, routing algorithms have been used to optimize evacuation routes, suggest re-routing (if needed), and aid emergency management in real-time decision-making [52] [53]. To perform evacuation re-routing, a Leaflet routing machine, a JavaScript library for interactive re-routing in web applications, was used to connect to the Graphhopper API. Graphhopper API provides various re-routing algorithms using the 'alternative_route' algorithm, which generates multiple alternative routes for a given start and end point. The Grasshopper API was then integrated into the prototype to calculate the shortest or alternative routes between multiple points. The parameters passed to the API include the algorithm type (alternative_route), maximum number of routes (max_paths), maximum weight factor (max_weight_factor), and maximum sharing factor (max_share_factor). The key parameters used in Graphhopper API for our user case are:

- Algorithm Type (alternative_route): This parameter specifies the algorithm used for routing, with alternative_route being particularly useful for evacuation as it provides several route options.

- Maximum Number of Routes (max_paths): Determines the number of alternative routes to generate. In evacuation scenarios, having multiple paths ensures that there are options available if the primary route becomes impassable.
- Maximum Weight Factor (max_weight_factor): This parameter influences the maximum weight of the alternative paths, which can be interpreted as a measure of route efficiency in terms of distance.
- Maximum Sharing Factor (max_share_factor): This parameter controls the degree of similarity between the alternative routes. A lower sharing factor will indicate the algorithm to provide routes that diverge from each other, which can increase the chances of avoiding blocked areas.

These parameters ensure that multiple evacuation routes are generated and that flooded areas are avoided as much as possible. After the API returned the routes, each route was checked to see if it was in the inundation area or not. The fastest route, which was out of the inundation area, was selected and displayed on the map to guide citizens toward a safe evacuation.

5.6. Deployment Into Cloud Platform

The flood evacuation tool is developed as a website so that it can be accessible remotely. We have used Advanced Cyberinfrastructure Coordination Ecosystem: Services

& Support (ACCESS), which is a program facilitated by NSF to provide cloud computing resources. Through the ACCESS program, we have used a virtual machine provided by Jetstream2 [54]. Jetstream is a cloud computing environment that was developed by Indiana University (IU) and funded by the National Science Foundation (NSF). Jetstream allows researchers to create virtual machines (VMs) that can be configured and scaled according to the needs of their projects. Our tool is also set up in a remote virtual machine (VM), which makes our tool remotely accessible through a website.

5.6 HAC Workflow for flood evacuation decision

This sub-section explains each method used in this research in detail. Figures 5.1 and 5.2 illustrate a brief step-by-step methodology of the HAC for flood evacuation decisions. In Step 1, we forecasted the gauge height of the river using (i) the LSTM model, (ii) the NWS AHPS forecast, and (iii) the Rational (deterministic) method. In the second step, we use the forecasted gauge height to map inundation areas. This inundation extent was created using a terrain-based river hydraulic model, i.e., the HAND method. In the third step, we collected X posts from X API, followed by step 4, which was X Text Classifier using BERT. Steps 3 and 4 helped collect human data. Finally, in the final step, we added the transportation network, evacuation re-routing scheme, and evacuation zones to the map. Each component was explained in detail in Figures 5.1 and 5.2. Figure 5.3 is the HAC flood evacuation tool architecture.

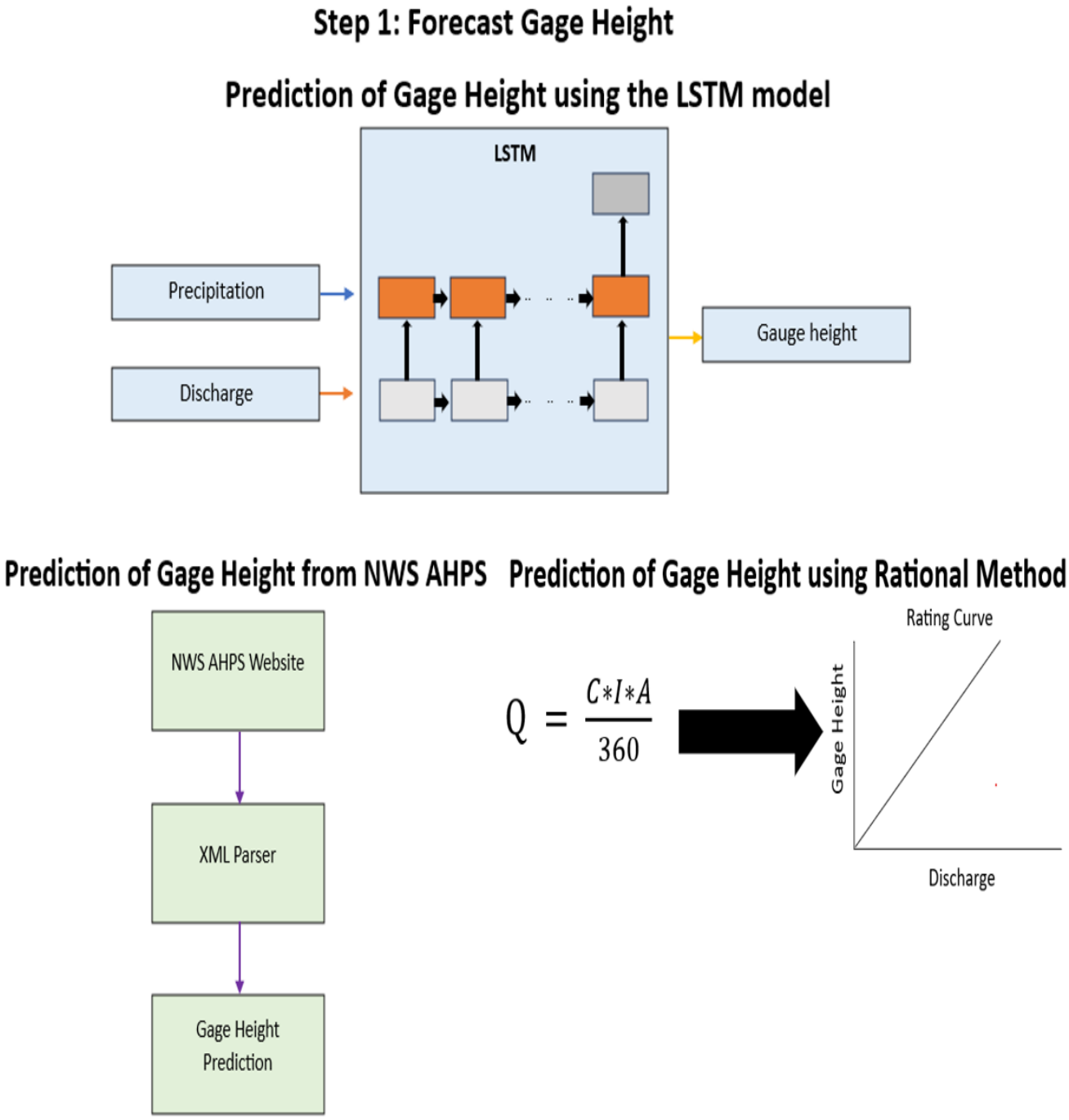

Figure 5.2. The workflow of gauge heigh prediction (step 1 of the proposed methodology).

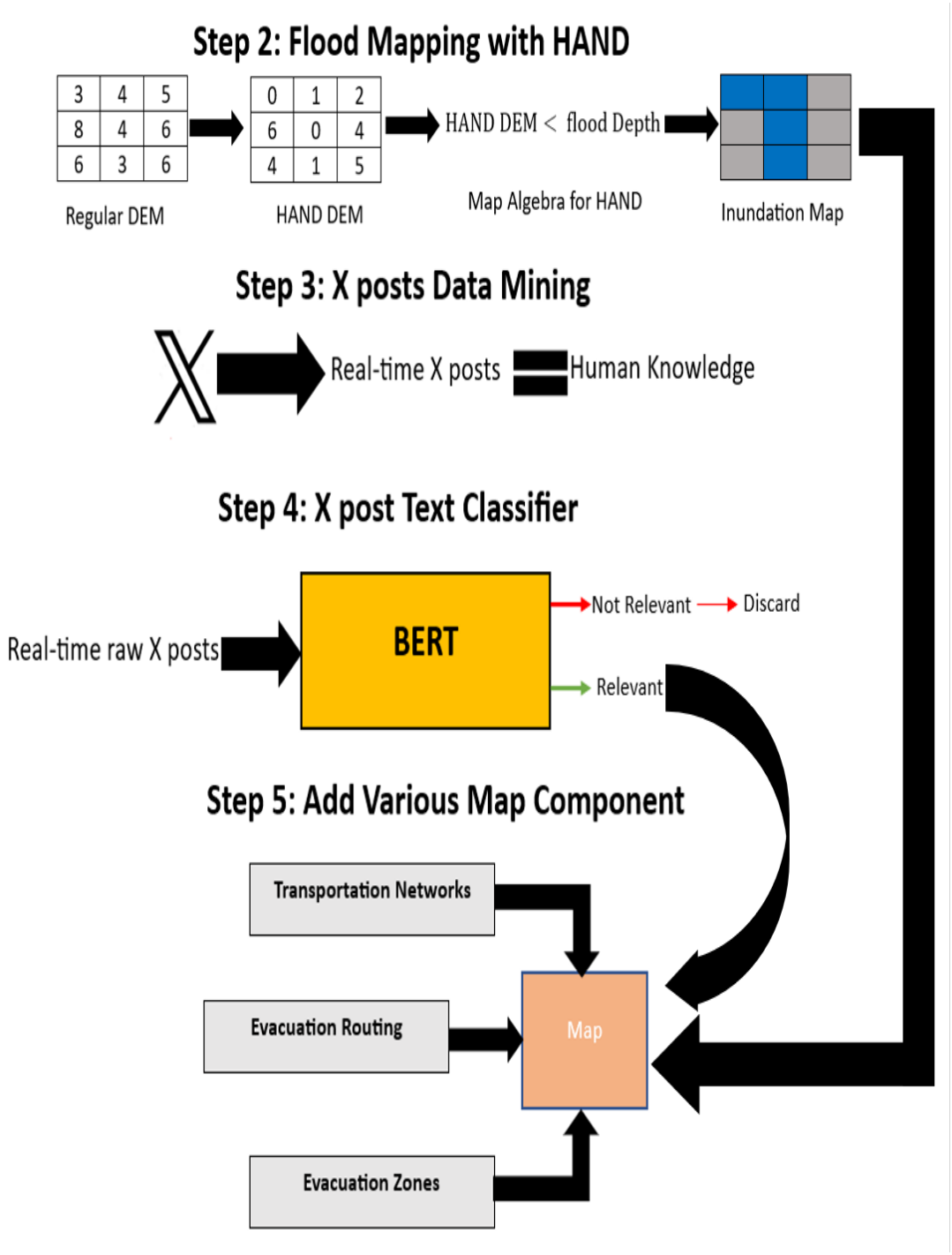

Figure 5.3. The workflows of flood inundation mapping and social media data collection (steps 2 to 5 of the proposed methodology).

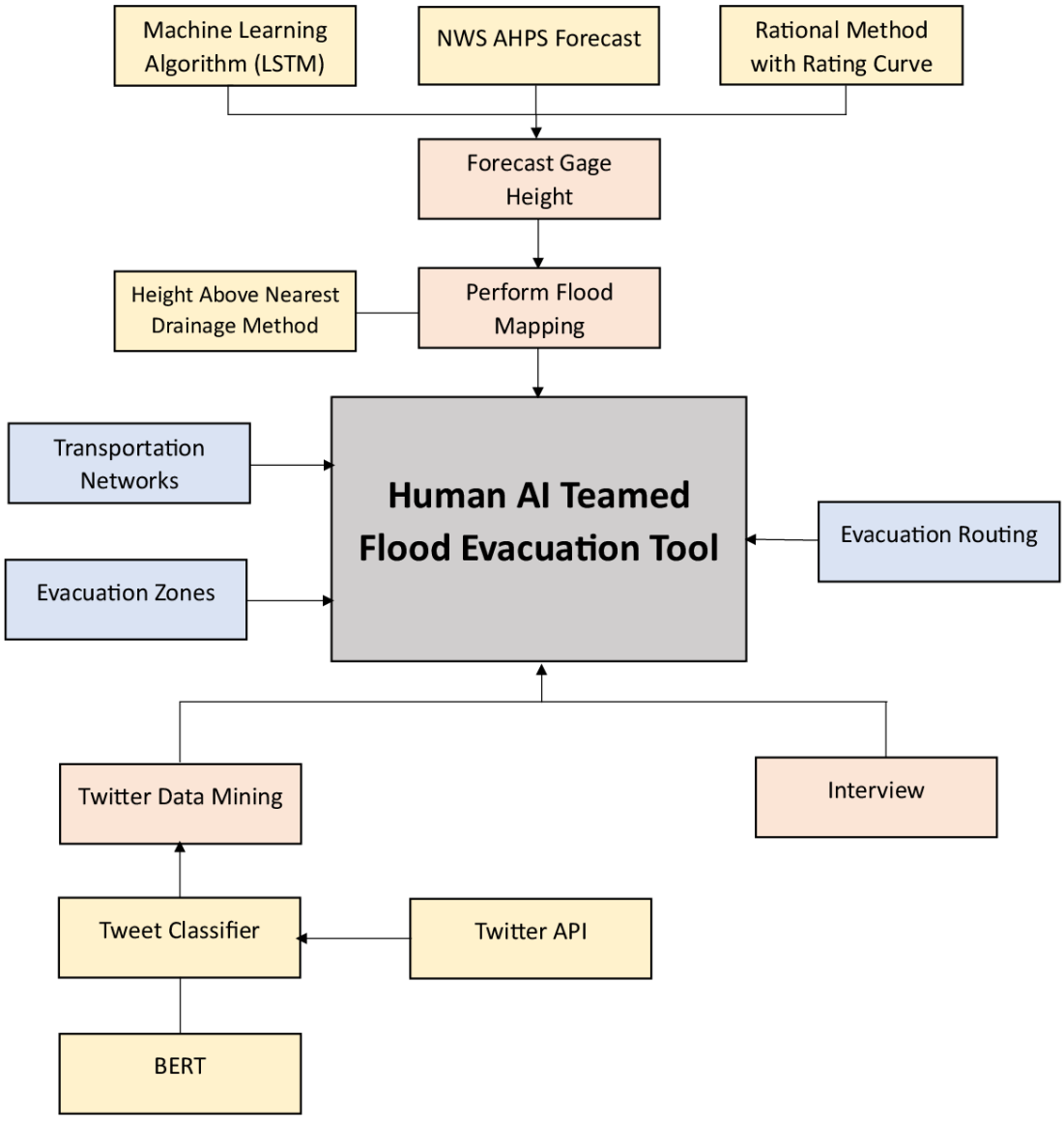

Figure 5.3. The overall workflow of HAC flood evacuation tool architecture.

CHAPTER SIX

RESULTS AND FINDINGS

This dissertation research focuses on using multiple approaches such as data-driven gauge height prediction, inundation mapping, and utilizing human data through X posts to predict flood events and suggest re-routing for evacuation decisions in the Lowcountry region of SC. This study shed light on potential synergies between machine learning, human data, traditional hydrological forecasting techniques and evacuation re-routing.

The traditional methods of predicting floods need to be more adaptable to handle changing conditions, which makes them less useful. We made our developed approaches more versatile and flexible in many ways to enhance the accuracy of flood forecasts as well as evacuation re-routing. Several data-driven methods were used to predict floods and improve the accuracy of evacuation decisions in real-time. Specifically, we used machine learning algorithms to predict gauge height, the HAND model to map flood inundation, a graphhopper API to suggest evacuation re-routing and the X API to get human data and validate the forecast. By using these methods together, we were able to make a flood forecasting tool that accurately uses the forecast to compute flood inundation extent and suggest evacuation re-routing. This new method is based on data, stressing the importance of accurate and up-to-date information. The model also considers people's thoughts and experiences, which helps it better understand how floods can affect citizens in real-time.

6.1 Human Data Analysis Results

In this research, we leveraged structured interviews and unstructured social media data to enrich the human dimension of our system. We conducted interviews with various organizations, which served as a foundation for comprehending what is needed in flood evacuation tools. These organizations had a profound experience in flood evacuation, and we gained enormous insights into the historical and operational challenges of flood evacuation decisions. During our interviews, we found that the stakeholders in the region lack the proper tools to assess flood evacuation decisions intelligently. The stakeholders needed a tool or a model that intelligently transferred domain knowledge of a river system into actionable insights, which was the most critical part of the flood evacuation tools. To bridge this gap, we created an action item to incorporate inundation methodology into our flood evacuation tool. More specifically, we added the HAND model for the inundation methodology to the pipeline. By adding the inundation methodology, we could translate this river's height into actionable insights, which would enhance the effectiveness of the flood evacuation tool. Other operational challenges were adding ground information through human knowledge. Getting human knowledge takes time and effort. However, the real-time nature of social media, especially X, is instrumental in adding real-time human knowledge to our system. The social media data provided immediacy and diversity of perspectives, offering contextual richness to incorporating human data into the flood evacuation tool.

We used X API to collect the X posts. X posts had to be filtered because they may or may not be related to flooding. This has been filtered via an X post-classifier model that has been constructed utilizing BERT. To develop an X post classifier model, a dataset of approximately 60000 X posts was gathered and manually annotated to indicate whether each X post was related to flooding or not. The X posts were partitioned into two sets, namely a training set and a test set, with a ratio of 75%:25%.

Figure 6.1 shows the architecture of the X post classifier. The input to the neural network is a text. The input dimension is “None” because in Keras of TensorFlow [55], a “None” dimension means that it can be any scalar number. So, the input dimension is arbitrary to the input text length. A preprocessed layer obtained from a pre-existing saved text preprocessing layer is utilized for BERT in TensorFlow Hub. The aforementioned layer serves as a companion to BERT models, facilitating the preprocessing of plain text inputs into the specific input format that BERT requires. The preprocessed layer's output is linked to the input of the BERT encoder layer sourced from a pre-existing TensorFlow Hub model that was trained beforehand. BERT utilizes a Transformer architecture and a deep, pre-trained neural network to generate dense vector representations for natural language. The present model employs 12 hidden layers, also known as Transformer blocks, with a hidden size of 768 and 12 attention heads. The weights utilized in this model correspond to those disclosed by the primary authors of BERT. The outputs of the encoder consist of two components: the "pooled_output," which serves to encapsulate the entirety of the input sequence, and the "sequence_output," which represents each individual token

within the context of the sequence. The output obtained from pooling is linked to the dropout layer with a rate of 0.1. The dropout is subsequently linked to a densely connected output layer.

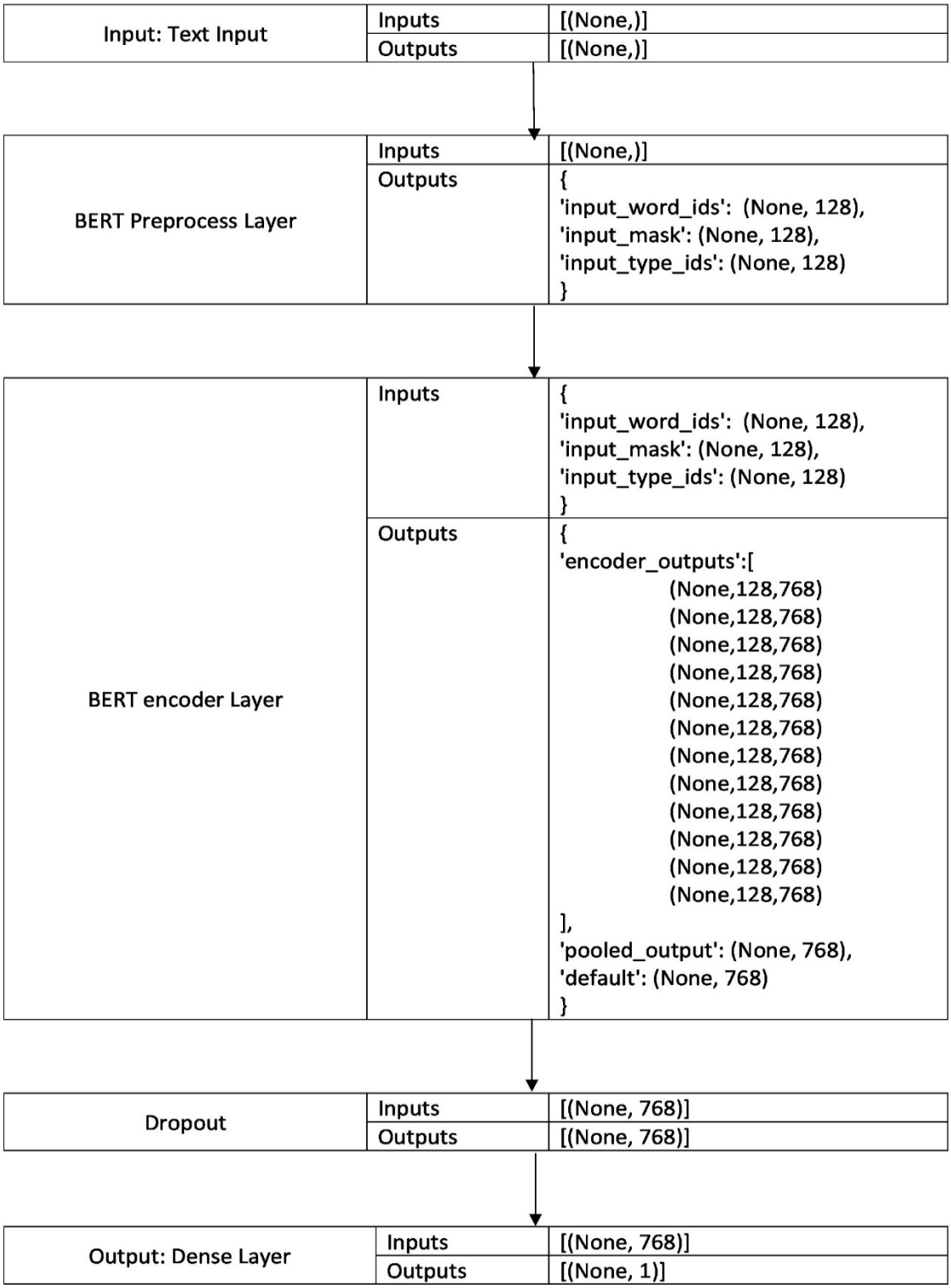

Figure 6.1. Neural network architecture of X post classifier constructed in this research.

The BERT model attained an accuracy rate of 88.5% along with a precision rate of 0.84% and a recall rate of 0.85% during the training phase. Similarly, during the testing phase, the model achieved an accuracy rate of 89%, a precision rate of 81%, and a recall rate of 94%.

Table 6.1: Confusion Matrix for the test set of the BERT model.

		Predicted Values	
		Negative	Positive
Actual Value	Negative	8183	1238
	Positive	319	5209

BERT's architecture, especially its bidirectional mechanism, was pivotal in understanding the context behind each X post. X posts were classified more accurately using this method. When examining the real-time application of BERT, its performance highlights the model's ability to effectively utilize human-generated data in the context of evolving flood situations. BERT demonstrates its efficacy as a vital tool for contemporary flood prediction systems by efficiently eliminating extraneous data and focusing on relevant flood-related information.

6.2 Flood Forecasting Results

We conducted training for both the LSTM and GRU models. To optimize and select the most optimal model, we employed Optuna. A total of 240 models were trained using the Optuna framework, from which the top four models were selected. The four stations that we used were 02173500, 02173000, 0212035 and 02110550. The performance of both the LSTM and GRU models exhibited a high degree of similarity. However, the LSTM model exhibited slightly superior performance, particularly on the test dataset. LSTM was particularly successful in capturing flood peak rates and time to peak, which are two important factors for flood emergency decisions.

Tables 6.2, 6.3 and 6.4 illustrate the performance achieved by LSTM in the test, validation and train set, respectively, for USGS02173500 (Turkey Creek River), USGS02173000 (South Fork Edisto River), USGS0212035 (North Fork Edisto River), and USGS02110550 (Waccamaw River).

Table 6.2. LSTM performance in test data set.

Station	MASE	NSE	Huber Loss	MSE	MAE
USGS02173500	0.0019	0. 9792	0.0120	0.02404	0. 1284
USGS02173000	0.0066	0.9832	0. 0248	0.0498	0.1619
USGS0212035	0.00460	0.98093	0.0177	0.0354	0.1406
USGS02110550	0.0122	0.9763	0.0067	0. 01356	0.09676

Table 6.3. LSTM performance in validation data set.

Station	MASE	Huber Loss	MSE	MAE
USGS02173500	0.0027	0.0070	0.0140	0.0887
USGS02173000	0.0052	0.0075	0.0150	0.0634
USGS0212035	0.0078	0.0065	0.0131	0.0696
USGS02110550	0.0063	0.0029	0.0058	0.0543

Table 6.4. LSTM performance in training data set.

Station	MASE	Huber Loss	MSE	MAE
USGS02173500	0.0028	0.0025	0.0050	0.0430
USGS02173000	0.0063	0.0020	0.0040	0.0447
USGS0212035	0.0094	0.0188	0.0890	0.0066
USGS02110550	0.0054	0.0067	0. 01356	0.09676

Figures 6.2, 6.3 and 6.4 show the actual vs predicted gauge height values. These figures also include discharge and precipitation for USGS02173500 (Turkey Creek River), USGS02173000 (South Fork Edisto River), USGS0212035 (North Fork Edisto River), and USGS02110550 (Waccamaw River) respectively.

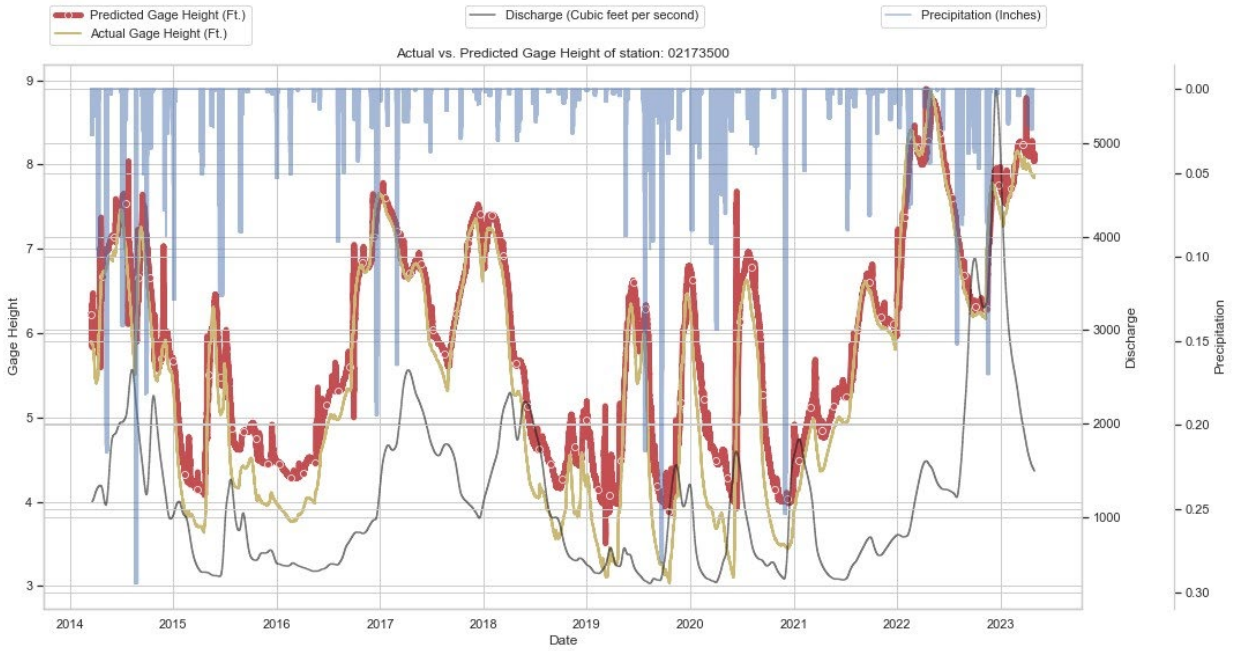

Figure 6.2. Flood gauge height prediction for USGS02173500.

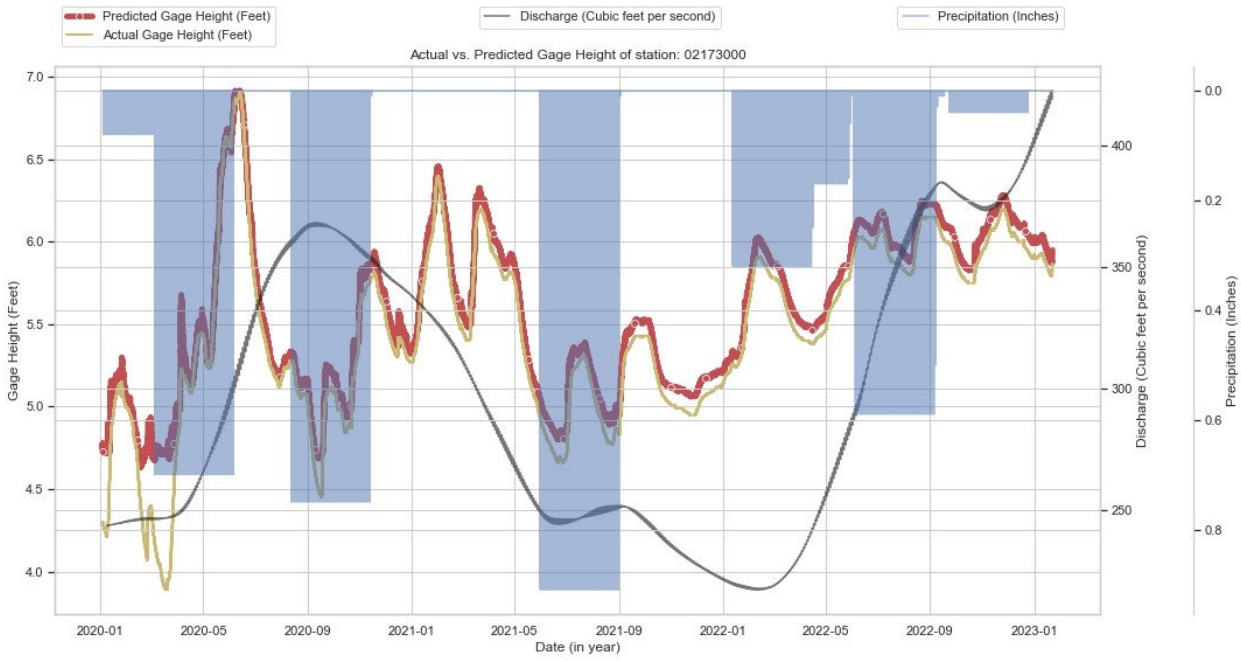

Figure 6.3. Flood gauge height prediction for USGS02173000.

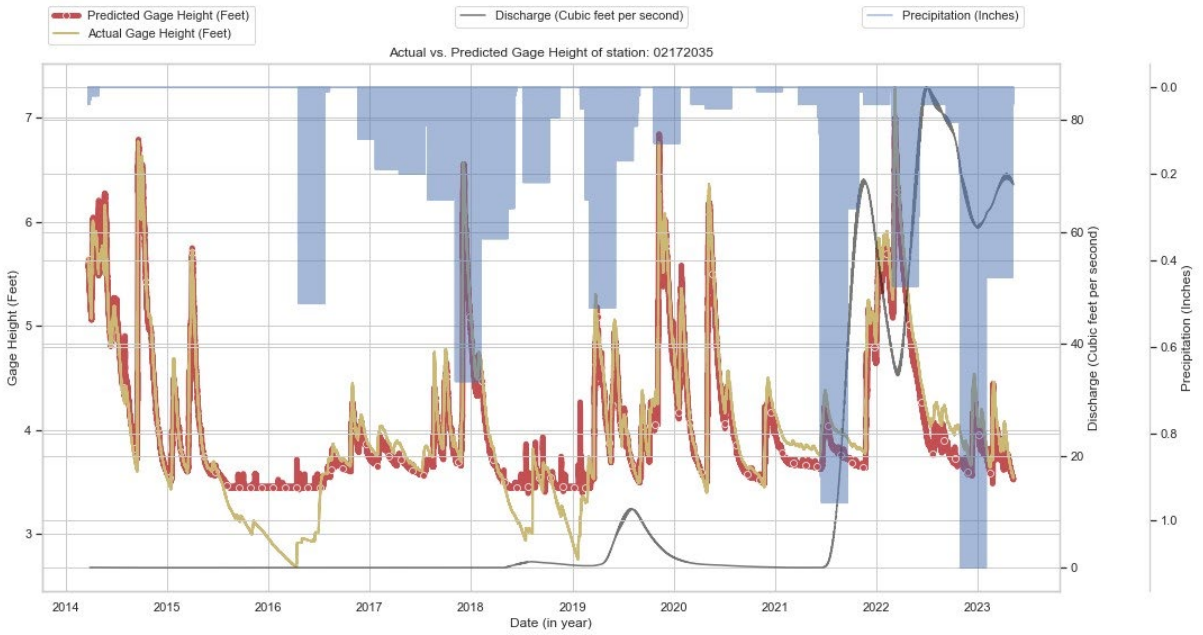

Figure 6.4. Flood gauge height prediction for USGS0212035

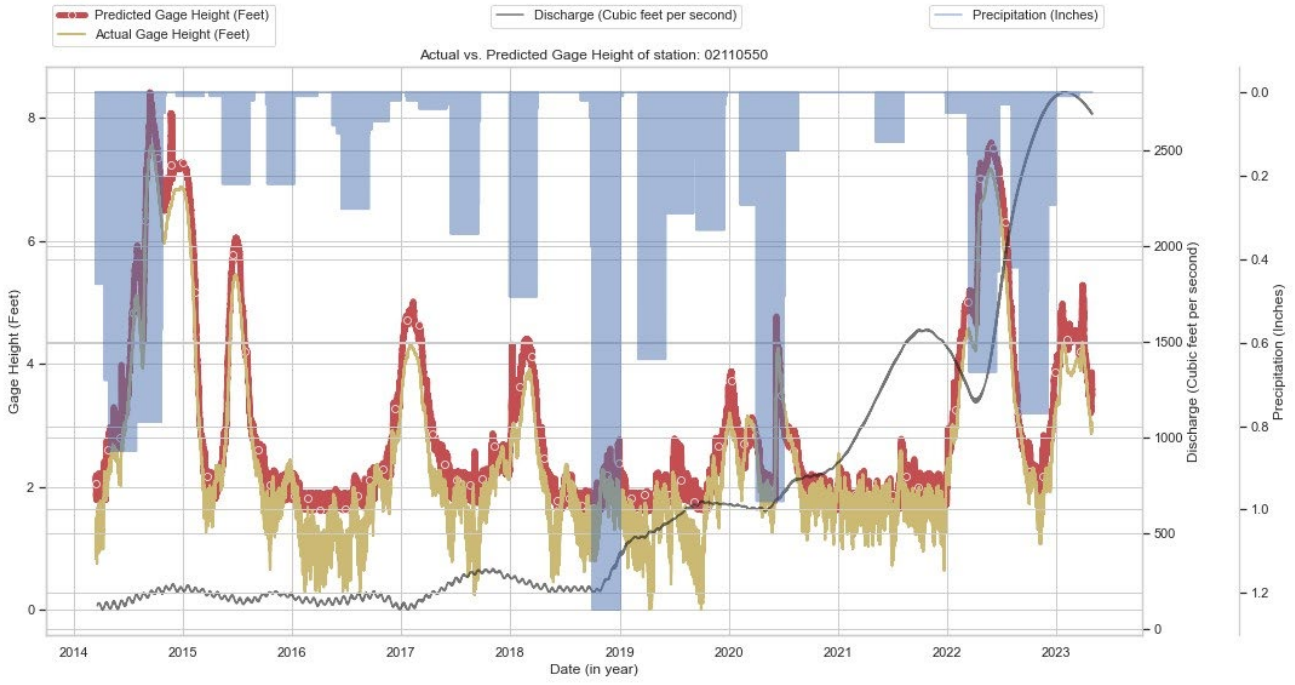

Figure 6.5. Flood gauge height prediction for USGS 02110550

6.3 Evacuation Re-routing Results

It is vital to include geospatial technologies and advanced routing algorithms to enhance evacuation planning. To suggest alternative routes, a Leaflet routing machine (through Graphhopper API) was employed for evacuation re-routing. We used 'alternative_route' as a parameter to the algorithm in Graphhopper API. Using this parameter, the API returns multiple routes; the best route that is not inundated was selected. When the API returned the route data, each path was checked if it was in a flooded area or not and the fastest route, which was far away from the inundation area was selected. The optimal route — the fastest one clear of flooding — was then displayed on the map to offer a reliable guide for safe evacuation. By actively avoiding inundated areas, the system ensures that the evacuation routes remain as safe as possible. The integration of real-time re-routing methods has substantially enhanced the safety and efficiency of emergency situations.

Figure 6.6. Map showing re-routed path from the inundated area.

CHAPTER SEVEN

CONCLUSION

The flood evacuation tool, which was created as an HAC prototype in this study, exhibits a high degree of efficacy in its ability to forecast river gauge height and suggest re-routing by combining LSTM and a river hydraulic model with relevant social media information and a re-routing approach that can facilitate disaster response and evacuation efforts. The incorporation of social media data provides a humanistic aspect to the developed HAC prototype and facilitates the identification of regions that may require prompt aid. The utilization of the HAND algorithm for inundation mapping and Graphhoper API for re-routing yields precise outcomes for an at-risk region for flooding. In general, the prototype exhibits significant potential for utilization in disaster response and evacuation endeavors within low-lying regions of South Carolina and other flood-prone areas. The high accuracy and precision achieved by the LSTM and BERT models demonstrate the effectiveness of machine learning and NLP in predicting river gauge height and filtering relevant social media data to validate flood prediction.

Traditionally, machine learning models rely on historical data to make predictions, but this approach may need to be revised in unpredictable circumstances like flooding, where real-time information is critical. To address this challenge, we introduced a new methodology incorporating machine learning predictions and human expertise derived

from X data into a geographical representation. The cartographic representation functions as an interface between machine learning and human inputs, facilitating mutual reinforcement and enhancing the precision of predictions. Utilizing X data enables the acquisition of contemporary human knowledge, augmenting machine learning models' predictive capacity. The integration of two sources of information is facilitated by utilizing a visualization map as a platform, resulting in creating a cohesive perspective of the situation. This methodology enables instantaneous cooperation between human specialists and the machine learning algorithm, resulting in enhanced precision and efficacy of predictions in emergency scenarios. This HAC strategy is the first step towards achieving human-AI collaboration in flood evacuation problems. As applied to flood management and planning, the human AI collaboration strategy centers on leveraging extant competencies to strategically coordinate the interplay between human data and machine learning prediction systems to achieve optimal disaster response outcomes. This involves a range of activities, including but not limited to information reception and transmission, situational awareness maintenance, and interview data to understand the needs and attitudes of stakeholders. The utilization of human-AI collaboration in the context of flood emergency management has the potential to augment human capabilities and knowledge, thereby increasing overall effectiveness. The present collaboration involves high-risk teaming, wherein ultimate decision-making authority rests with humans.

AI continues to evolve, and its decision-making and prediction can help teams deal with real-time planning during flood emergencies. AI is vital to resilience in flood

evacuation response. Still, with careful coordination with humans, this teaming paradigm may achieve the necessary scope and scale and adversely impact at-risk populations. One way to help the stakeholders (for example, emergency responders, transportation officials, and public safety staff) better understand and trust AI prediction is to provide them with a proof of concept using data from prior disasters. If these officials can verify the accuracy of the black box with known data, this can help to demonstrate the value that AI machines can have during an actual disaster event. However, finding ways to improve trust in human-AI interaction is essential for emergency officials to be willing to use HAC systems when lives are on the line.

Societal demands for flood management and decision-making inquiry and problem-solving will continue to increase the need for technologies such as HAC in prediction and planning. Engineering solutions to flooding management problems, including evacuation and warning, real-time decision-making increasingly rely on sophisticated computational solutions rather than manual/ empirical assessment. At the same time, scientists working in the field of AI and flood emergencies will increasingly be pushed towards inquiry directly relevant to societal decision-making, bolding human factors in AI forecasting, which has important consequences for people's safety and protection. However, more research is needed to develop methods for incorporating human data and supporting trust in HAC during evacuation responses that consider flood situational conditions and inform emergency officials of when to rely on an AI system and when to intervene. This research will serve as a foundation for future studies exploring the potential of human-AI

collaboration approaches in flood disaster domains. The application of this approach could be extended to other fields, such as healthcare, transportation, and security, where decision-making is critical and requires real-time data. Exploring and refining the HAC approach could unlock new possibilities for improving trust and achieving more significant breakthroughs in various HAC domains.

APPENDICES

Appendix A

Pseudocode

Pseudocode 1: Calculate HAND from DEM

requires: flood_depth, TL, BR, hand_DEM_path

```
hand_dataset <- OPEN_GIS_DATASET(hand_DEM_path)
band <- GET_BAND(hand_dataset, 1)

transform <- GET_DATASET_GEOTRANSFORM(hand_dataset)
inv_transform <- CALCULATE_INVERSE_GEOTRANSFORM(transform)

top_left_pixel <- APPLY_INVERSE_GEOTRANSFORM(inv_transform, TL.longitude, TL.latitude)
bottom_right_pixel <- APPLY_INVERSE_GEOTRANSFORM(inv_transform, BR.longitude, BR.latitude)

start_x <- MAX(0, INT(MIN(top_left_pixel.x, bottom_right_pixel.x)))
end_x <- MIN(GET_DATASET_WIDTH(hand_dataset), INT(MAX(top_left_pixel.x, bottom_right_pixel.x)) + 1)
start_y <- MAX(0, INT(MIN(top_left_pixel.y, bottom_right_pixel.y)))
end_y <- MIN(GET_DATASET_HEIGHT(hand_dataset), INT(MAX(top_left_pixel.y, bottom_right_pixel.y)) + 1)

hand_array_clipped <- READ_RASTER_DATA_AS_ARRAY(band, start_x, start_y, width <- end_x - start_x, height <- end_y - start_y)

no_data_value <- GET_BAND_NO_DATA_VALUE(band)
IF no_data_value IS NOT NONE:
  REPLACE_ARRAY_VALUES(hand_array_clipped, no_data_value, NaN)

inundated_mask <- CREATE_MASK_WHERE(hand_array_clipped IS LESS OR EQUAL TO flood_depth AND NOT NaN)

bins <- DEFINE_BINS([0, 0.5, 1, 1.5, 2], flood_depth)

zone_indices <- ASSIGN_TO_BINS(hand_array_clipped[WHERE inundated_mask], bins)

Zone1, Zone2, Zone3, Zone4, Zone5 <- INITIALIZE_EMPTY_LISTS()
lat_list, lon_list <- INITIALIZE_EMPTY_LISTS()

FOR zone_number FROM 1 TO LENGTH(bins) + 1:
  zone_mask <- IDENTIFY_MASK_FOR_ZONE(zone_indices, zone_number)
  IF zone_mask CONTAINS TRUE VALUES:
    inundated_indices <- GET_TRUE_INDICES(inundated_mask)
    selected_indices <- FILTER_INDICES_BY_ZONE(inundated_indices, zone_mask)
    world_coords <- CONVERT_PIXELS_TO_WORLD_COORDINATES(selected_indices, transform, start_x, start_y)
    APPEND_ZONE_COORDINATES(Zone{zone_number}, world_coords)
    APPEND_LAT_LON_FROM_COORDINATES(lat_list, lon_list, world_coords)

FOR zone_number FROM LENGTH(bins) + 1 TO 5:
  CLEAR_ZONE_LIST(Zone{zone_number})

RETURN Zone1, Zone2, Zone3, Zone4, Zone5, lat_list, lon_list
```

This pseudocode1 requires flood depth (flood_depth), top left clipped rectangle coordinate (TL), bottom right clipped rectangle coordinate (BR) and HAND DEM path (hand_DEM_path). Functions used in this pseudo-code:

- OPEN_GIS_DATASET represents the process of opening the GIS file.
- GET_BAND, GET_DATASET_GEOTRANSFORM, and similar functions represent various GIS data operations.
- CALCULATE_INVERSE_GEOTRANSFORM calculates the inverse geotransformation matrix.
- APPLY_INVERSE_GEOTRANSFORM applies the inverse geotransform to convert world coordinates to pixel coordinates.
- READ_RASTER_DATA_AS_ARRAY reads raster data from the GIS file into a numeric array.
- REPLACE_ARRAY_VALUES replaces specific values in an array with another value.
- CREATE_MASK_WHERE creates a boolean mask based on a condition.
- DEFINE_BINS, ASSIGN_TO_BINS, and IDENTIFY_MASK_FOR_ZONE are used for categorizing the data into different zones based on the flood depth.
- CONVERT_PIXELS_TO_WORLD_COORDINATES converts pixel coordinates back to world.

Pseudocode 2: Forecast gauge height in real-time

requires: flood_station, period, scaler_path, model_path

```
TRY:
   herring <- NWIS_WEB_SERVICE(flood_station, 'iv', period)
   data <- EXTRACT_AND_PROCESS_DATA(herring)
CATCH Exception:
   HANDLE_DATA_RETRIEVAL_ERROR(flood_station)
   RETURN NONE

scaler <- LOAD_SCALER(scaler_path)
scaled_data <- PREPARE_DATA_FOR_PREDICTION(data, scaler)

custom_objects <- SETUP_MODEL_CUSTOM_OBJECTS()
regressor <- LOAD_MODEL(model_path, custom_objects)

prediction <- regressor.PREDICT(scaled_data)

inversed_gage_height <- POST_PROCESS_PREDICTIONS(prediction, scaler)

df_predictions <- PREPARE_PREDICTIONS_DATAFRAME(inversed_gage_height, data)

RETURN df_predictions
```

Pseudocode 2 requires identifier for the flood station (flood_station), time period over which to fetch data (period), path to the directory where the scaler files are stored (scaler_path) and path to the directory where the trained machine learning model files are stored (model_path). Function used in this pseudocode are:

- NWIS_WEB_SERVICE: Uses NWIS API to perform GET request and fetch data from it.
- EXTRACT_AND_PROCESS_DATA: Performs operations like fetching data, resampling, and timezone localization.
- HANDLE_DATA_RETRIEVAL_ERROR: Encapsulates error handling for data retrieval issues.
- LOAD_SCALER: Loads and returns scaler.

- PREPARE_DATA_FOR_PREDICTION: Prepares data scaling and preparation for input into the predictive model.
- LOAD_MODEL: Loads and return machine learning model.
- PREDICT: Predict and return predicted data.
- SETUP_MODEL_CUSTOM_OBJECTS: Represents the setup for custom objects required by the model, such as custom loss functions or metrics.
- POST_PROCESS_PREDICTIONS: Performs the post-processing of predictions to convert them from the scaled form back to the original measurement scale.
- PREPARE_PREDICTIONS_DATAFRAME: Prepares the creation of a DataFrame with predictions, including setting up the index with appropriate timestamps.

Appendix B

Training data

The upcoming subsections, includes the training data done to hypertune the parameter using Optuna. We have trained 240 models to select the best 4 for this research. The trial which was selected is highlighted. In this subsection the following notations are used:

- Trial is used as T.
- Units in 1st layer is used as L1.
- Units in 2nd layer is used as L2.
- Units in 3rd layer is used as L3.
- Units in 4th layer is used as L4.
- Units in 5th layer is used as L5.
- Units in 6th layer is used as L6.
- Dropout rate is used as DR.
- Epoch Number is used as EN.
- Validation Huber Loss is used as VHL.
- Validation Mean Square Error is used as VMSE.
- Validation Mean Absolute Error is used as VMAE.
- Validation Mean Absolute Scaled Error is used as VMASE.

LSTM model trainings for USGS02110550

T	L1	L2	L3	L4	L5	L6	DR	EN	VHL	VMSE	VMAE	VMASE	HL	MSE	MAE	MASE
0	133	93	77	50	30	12	0.1	82	0.0062	0.0125	0.0909	0.0056	0.0060	0.0119	0.0725	0.0063
1	128	149	107	60	37	7	0.19	176	0.0093	0.0187	0.0950	0.0053	0.0094	0.0188	0.0937	0.0063
2	127	103	72	66	23	15	0.36	129	0.0045	0.0090	0.0764	0.0056	0.0022	0.0044	0.0485	0.0062
3	177	81	96	68	17	5	0.11	65	0.0121	0.0241	0.1129	0.0054	0.0110	0.0222	0.1035	0.0063
4	107	126	80	58	20	9	0.38	140	0.0044	0.0088	0.0705	0.0054	0.0029	0.0058	0.0543	0.0063
5	136	100	74	48	18	7	0.14	89	Model pruned							
6	161	83	52	70	13	13	0.13	79	Model pruned							
7	166	110	76	51	32	8	0.31	113	Model pruned							
8	152	85	98	58	26	13	0.33	194	Model pruned							
9	161	138	70	42	21	6	0.44	179	Model pruned							
10	100	127	56	32	11	10	0.44	140	Model pruned							
11	103	118	86	62	24	15	0.37	137	Model pruned							
12	125	129	63	64	26	10	0.39	116	Model pruned							
13	113	109	87	57	19	15	0.5	149	Model pruned							
14	116	155	65	65	15	9	0.24	160	Model pruned							
15	143	139	85	55	22	12	0.25	108	Model pruned							
16	114	105	64	42	30	11	0.34	156	Model pruned							
17	196	121	96	54	39	9	0.27	131	Model pruned							
18	119	96	81	66	10	14	0.36	100	Model pruned							
19	106	118	69	44	34	11	0.29	54	Model pruned							
20	137	137	58	61	23	8	0.41	124	Model pruned							
21	127	92	77	50	29	13	0.21	93	Model pruned							
22	136	93	80	34	27	12	0.3	75	Model pruned							
23	147	103	71	47	20	14	0.17	164	Model pruned							
24	126	113	91	38	29	11	0.33	123	Model pruned							
25	109	89	80	53	33	14	0.26	141	Model pruned							
26	120	100	90	70	15	9	0.23	103	Model pruned							
27	132	126	73	57	24	12	0.3	85	Model pruned							

28	143	114	67	63	28	10	0.18	148	Model pruned
29	122	133	107	59	35	7	0.35	182	Model pruned

LSTM model trainings for USGS02172035

T	L1	L2	L3	L4	L5	L6	DR	EN	VHL	VMSE	VMAE	VMASE	HL	MSE	MAE	MASE
0	151	88	54	70	26	11	0.3	191	0.0215	0.0430	0.1413	0.0066	0.0128	0.0259	0.0968	0.0078
1	169	140	76	58	36	12	0.14	166	0.0121	0.0242	0.1020	0.0066	0.0108	0.0220	0.0947	0.0082
2	163	123	69	67	35	14	0.23	117	0.0094	0.0188	0.0890	0.0066	0.0065	0.0131	0.0696	0.0078
3	110	140	101	55	16	13	0.13	60	0.0161	0.0322	0.1189	0.0066	0.0206	0.0427	0.1354	0.0086
4	140	96	62	60	10	14	0.24	87	0.0147	0.0294	0.1063	0.0066	0.0101	0.0204	0.0917	0.0080
5	194	122	73	52	26	7	0.15	88	Model pruned							
6	127	152	81	47	16	14	0.38	89	Model pruned							
7	196	108	57	58	32	10	0.23	173	Model pruned							
8	130	98	54	59	31	15	0.26	134	Model pruned							
9	121	156	86	47	31	14	0.23	96	Model pruned							
10	167	119	108	32	40	8	0.49	130	Model pruned							
11	167	137	69	70	39	12	0.11	156	Model pruned							
12	173	132	90	64	35	10	0.17	156	Model pruned							
13	183	120	71	65	36	5	0.17	118	Model pruned							
14	153	146	92	38	22	12	0.19	151	Model pruned							
15	158	130	65	64	35	15	0.14	184	Model pruned							
16	180	110	77	41	29	12	0.1	112	Model pruned							
17	141	144	80	51	22	9	0.2	200	Model pruned							
18	161	128	63	67	37	13	0.18	52	Model pruned							
19	184	111	97	56	33	11	0.29	143	Model pruned							
20	145	149	50	61	28	13	0.1	170	Model pruned							
21	136	80	62	61	10	14	0.26	105	Model pruned							
22	104	99	68	54	10	15	0.34	80	Model pruned							
23	173	99	76	61	15	13	0.22	123	Model pruned							

24	147	91	60	65	21	14	0.15	73	Model pruned
25	160	125	84	48	19	11	0.24	103	Model pruned
26	137	114	74	68	13	12	0.2	66	Model pruned
27	170	139	67	58	38	15	0.27	137	Model pruned
28	154	135	58	62	29	14	0.22	172	Model pruned
29	188	104	50	69	25	11	0.31	115	Model pruned

LSTM model training for USGS02173000

T	L1	L2	L3	L4	L5	L6	DR	EN	VHL	VMSE	VMAE	VMASE	HL	MSE	MAE	MASE
0	153	124	55	41	22	12	0.17	138	0.0092	0.0185	0.0665	0.0050	0.0019	0.0038	0.0426	0.0062
1	102	115	57	51	33	9	0.39	59	0.0064	0.0128	0.0605	0.0053	0.0024	0.0049	0.0462	0.0062
2	149	92	108	67	15	5	0.12	200	0.0028	0.0056	0.0464	0.0053	8.7537e-04	0.0018	0.0302	0.0061
3	102	100	52	31	11	6	0.18	185	0.0030	0.0059	0.0461	0.0053	0.0022	0.0045	0.0424	0.0061
4	200	117	57	45	31	12	0.15	72	0.0110	0.0220	0.0712	0.0051	0.0021	0.0042	0.0443	0.0062
5	177	110	79	34	14	14	0.34	64	Model pruned							
6	101	139	83	39	31	13	0.45	109	Model pruned							
7	200	85	69	31	20	8	0.18	176	Model pruned							
8	105	150	92	40	18	5	0.2	64	Model pruned							
9	184	129	70	65	16	15	0.36	138	Model pruned							
10	137	80	105	70	39	7	0.27	194	Model pruned							
11	129	99	110	57	10	5	0.1	198	Model pruned							
12	156	97	94	57	10	7	0.1	167	Model pruned							
13	125	97	98	60	14	5	0.25	165	Model pruned							
14	165	104	69	50	25	10	0.22	108	Model pruned							
15	115	88	84	69	13	7	0.14	184	Model pruned							
16	140	91	75	49	23	6	0.23	153	Model pruned							
17	120	106	62	63	18	9	0.29	150	Model pruned							
18	142	92	88	35	10	6	0.22	182	Model pruned							

19	166	157	50	54	26	8	0.14	199	Model pruned							
20	116	128	101	44	13	10	0.19	114	Model pruned							
21	108	112	50	54	40	9	0.33	94	Model pruned							
22	110	117	63	46	35	11	0.41	87	Model pruned							
23	101	103	59	65	29	6	0.48	133	Model pruned							
24	131	111	65	30	36	8	0.31	160	Model pruned							
25	122	84	54	53	35	6	0.38	87	0.0075	0.0150	0.0634	0.0052	0.0020	0.0040	0.0447	0.0063
26	146	137	74	36	28	9	0.26	188	Model pruned							
27	112	93	110	49	17	5	0.32	121	Model pruned							
28	184	119	53	60	20	7	0.24	176	Model pruned							
29	154	125	58	42	23	11	0.16	144	Model pruned							

LSTM model training for USGS02173500

T	L1	L2	L3	L4	L5	L6	DR	EN	VHL	VMSE	VMAE	VMASE	HL	MSE	MAE	MASE
0	132	90	73	44	15	10	0.16	100	0.0070	0.0140	0.0887	0.0027	0.0025	0.0050	0.0430	0.0028
1	154	141	65	66	11	15	0.22	119	0.0133	0.0267	0.1202	0.0027	0.0135	0.0282	0.1061	0.0030
2	169	93	58	45	26	12	0.18	101	0.0124	0.0249	0.1172	0.0027	0.0105	0.0211	0.0990	0.0029
3	120	142	76	64	32	7	0.21	54	0.0131	0.0263	0.1261	0.0027	0.0135	0.0282	0.1066	0.0030
4	111	113	51	49	35	5	0.36	70	0.0097	0.0195	0.1012	0.0027	0.0110	0.0238	0.0931	0.0030
5	184	131	79	41	40	9	0.21	137	Model pruned							
6	196	137	81	41	36	10	0.38	53	Model pruned							
7	166	152	54	44	37	15	0.24	195	Model pruned							
8	154	103	100	69	11	15	0.35	118	Model pruned							
9	167	143	103	51	27	7	0.13	115	Model pruned							
10	134	83	90	57	17	12	0.48	160	Model pruned							
11	102	111	50	30	19	5	0.3	80	Model pruned							
12	124	120	66	53	20	5	0.11	83	Model pruned							
13	107	80	66	34	31	8	0.28	79	Model pruned							
14	136	100	93	56	22	12	0.34	94	Model pruned							

15	117	117	110	47	14	6	0.14	144	Model pruned
16	138	93	61	36	29	10	0.4	61	Model pruned
17	111	128	72	60	23	13	0.25	68	Model pruned
18	131	107	89	49	33	9	0.16	99	Model pruned
19	147	89	50	39	15	11	0.27	170	Model pruned
20	125	116	73	53	35	7	0.11	73	Model pruned
21	171	92	57	45	26	13	0.16	99	Model pruned
22	175	98	58	44	24	13	0.17	105	Model pruned
23	145	87	62	49	40	11	0.2	90	Model pruned
24	112	95	70	38	29	14	0.19	109	Model pruned
25	157	105	55	46	19	11	0.14	69	Model pruned
26	185	110	82	42	29	9	0.24	88	Model pruned
27	100	123	60	52	14	12	0.19	140	Model pruned
28	127	85	53	56	22	8	0.1	129	Model pruned
29	160	101	68	32	11	14	0.22	129	Model pruned

GRU model training for USGS02110550

T	L1	L2	L3	L4	L5	L6	DR	EN	VHL	VMSE	VMAE	VMASE	HL	MSE	MAE	MASE
0	161	106	101	64	39	5	0.43	51	0.2348	0.4820	0.6010	0.0104	0.2066	0.4534	0.5425	0.0079
1	123	139	103	50	14	13	0.19	77	0.0051	0.0102	0.0797	0.0052	0.0054	0.0108	0.0781	0.0063
2	169	120	53	41	33	8	0.11	125	0.0052	0.0103	0.0778	0.0055	0.0050	0.0099	0.0680	0.0062
3	113	83	52	55	22	10	0.36	74	0.0025	0.0050	0.0543	0.0056	0.0041	0.0082	0.0603	0.0062
4	129	112	55	61	30	15	0.16	153	0.0037	0.0074	0.0623	0.0051	0.0036	0.0072	0.0612	0.0062
5	127	152	72	51	18	15	0.42	169	Model pruned							
6	187	101	96	62	12	8	0.39	125	Model pruned							
7	198	91	95	66	26	12	0.37	168	Model pruned							
8	134	114	61	35	23	6	0.27	50	Model pruned							
9	135	140	66	61	12	10	0.41	94	Model pruned							
10	100	86	82	49	20	10	0.49	95	Model pruned							
11	105	83	51	56	30	15	0.29	194	Model pruned							

12	113	134	79	56	29	12	0.24	146	Model pruned
13	144	99	62	56	37	8	0.33	147	Model pruned
14	117	125	50	69	25	12	0.22	99	Model pruned
15	150	159	59	41	33	14	0.33	72	Model pruned
16	113	80	75	44	17	11	0.11	200	Model pruned
17	135	110	89	30	22	9	0.17	144	Model pruned
18	161	92	68	59	28	13	0.32	117	Model pruned
19	125	127	57	69	33	7	0.27	172	Model pruned
20	144	98	66	52	36	10	0.35	111	Model pruned
21	121	142	107	46	15	14	0.17	81	Model pruned
22	108	143	107	53	15	14	0.18	70	Model pruned
23	129	117	86	58	10	13	0.21	66	Model pruned
24	119	133	55	47	20	11	0.3	81	Model pruned
25	141	153	90	54	26	15	0.26	104	Model pruned
26	106	127	72	49	23	13	0.15	137	Model pruned
27	124	107	101	66	30	11	0.21	87	Model pruned
28	113	148	63	61	15	14	0.24	159	Model pruned
29	157	91	102	65	21	5	0.14	56	Model pruned

GRU model training for USGS02172035

T	L1	L2	L3	L4	L5	L6	DR	EN	VHL	VMSE	VMAE	VMASE	HL	MSE	MAE	MASE
0	169	115	64	62	26	5	0.42	121	0.0500	0.1002	0.2511	0.0066	0.0233	0.0484	0.1511	0.0072
1	115	113	58	59	30	10	0.13	83	0.0145	0.0290	0.1269	0.0066	0.0116	0.0246	0.0972	0.0078
2	142	93	94	32	12	9	0.49	186	0.0214	0.0427	0.1515	0.0066	0.0139	0.0291	0.1097	0.0077
3	127	85	108	34	35	5	0.11	197	0.0166	0.0333	0.1269	0.0066	0.0155	0.0326	0.1163	0.0082
4	189	104	70	60	25	5	0.23	114	0.0424	0.0848	0.2282	0.0066	0.0206	0.0440	0.1392	0.0075
5	165	111	107	50	25	13	0.24	141	Model pruned							
6	198	124	77	48	12	10	0.29	102	Model pruned							
7	156	154	54	31	11	15	0.12	183	Model pruned							
8	108	81	60	34	19	14	0.33	182	Model pruned							

9	184	90	78	44	10	14	0.35	83	Model pruned
10	100	134	51	68	39	8	0.18	52	Model pruned
11	125	141	94	41	37	7	0.1	152	Model pruned
12	128	102	109	57	32	7	0.15	70	Model pruned
13	120	126	91	55	31	12	0.18	157	Model pruned
14	139	84	86	39	34	11	0.11	92	Model pruned
15	112	97	101	65	28	6	0.17	52	Model pruned
16	136	110	70	54	20	9	0.21	200	Model pruned
17	115	154	84	70	36	11	0.14	135	Model pruned
18	100	138	101	50	30	7	0.1	73	Model pruned
19	152	120	70	37	40	9	0.25	168	Model pruned
20	131	88	58	44	21	11	0.15	107	Model pruned
21	141	94	99	30	34	9	0.49	197	Model pruned
22	147	100	94	35	14	10	0.5	181	Model pruned
23	122	81	106	34	16	8	0.4	169	Model pruned
24	131	90	87	46	22	6	0.2	133	Model pruned
25	160	107	98	40	28	12	0.27	191	Model pruned
26	145	96	104	30	17	10	0.14	170	Model pruned
27	108	117	110	37	33	8	0.21	155	Model pruned
28	133	87	82	62	36	6	0.27	66	Model pruned
29	118	114	74	58	28	5	0.47	119	Model pruned

GRU model training for USGS02173000

T	L1	L2	L3	L4	L5	L6	DR	EN	VHL	VMSE	VMAE	VMASE	HL	MSE	MAE	MASE
0	103	102	93	34	11	15	0.43	172	0.0083	0.0166	0.0818	0.0059	0.0063	0.0126	0.0823	0.0064
1	158	116	52	64	40	15	0.14	189	0.0138	0.0276	0.0972	0.0057	0.0130	0.0261	0.0930	0.0062
2	131	133	50	55	30	9	0.49	193	0.1260	0.2906	0.3362	0.0098	0.0655	0.1353	0.2582	0.0080
3	104	117	85	32	24	11	0.23	154	0.0114	0.0228	0.0696	0.0052	0.0015	0.0031	0.0384	0.0062
4	152	92	62	38	23	8	0.14	62	0.0070	0.0140	0.0601	0.0051	0.0022	0.0044	0.0446	0.0061
5	126	119	51	63	28	15	0.23	57	Model pruned							

6	115	90	63	59	28	9	0.37	91	Model pruned
7	198	99	76	68	18	14	0.48	51	Model pruned
8	181	94	66	42	11	10	0.27	193	Model pruned
9	180	111	97	48	31	7	0.34	61	Model pruned
10	150	153	72	41	21	5	0.12	111	Model pruned
11	146	80	107	31	10	12	0.39	153	Model pruned
12	164	102	89	38	15	7	0.18	148	Model pruned
13	136	135	97	47	37	12	0.1	93	Model pruned
14	105	84	62	36	16	7	0.3	137	Model pruned
15	169	106	109	30	22	13	0.43	172	Model pruned
16	139	134	83	44	35	8	0.18	122	Model pruned
17	119	91	94	53	19	5	0.31	86	Model pruned
18	157	106	70	37	13	10	0.41	170	Model pruned
19	174	157	57	35	25	12	0.35	76	Model pruned
20	196	98	103	40	14	8	0.44	111	Model pruned
21	106	127	82	33	23	11	0.23	159	Model pruned
22	100	113	87	30	25	14	0.25	172	Model pruned
23	117	126	77	34	19	11	0.2	134	Model pruned
24	109	145	88	45	26	6	0.15	182	Model pruned
25	123	107	93	33	33	9	0.26	161	Model pruned
26	143	84	80	39	17	13	0.15	146	Model pruned
27	130	121	101	51	21	10	0.21	122	Model pruned
28	110	93	85	43	13	8	0.17	104	Model pruned
29	151	114	57	37	39	15	0.14	181	Model pruned

GRU model training for USGS02173500

T	L1	L2	L3	L4	L5	L6	DR	EN	VHL	VMSE	VMAE	VMASE	HL	MSE	MAE	MASE
0	171	121	107	55	40	6	0.3	122	0.0038	0.0076	0.0654	0.0027	0.0041	0.0085	0.0551	0.0027
1	145	93	101	65	19	14	0.14	130	0.0099	0.0198	0.1033	0.0027	0.0063	0.0126	0.0790	0.0029
2	192	89	67	33	30	12	0.32	76	0.0184	0.0369	0.1401	0.0027	0.0175	0.0379	0.1158	0.0029

3	105	159	84	31	22	5	0.16	182	0.0079	0.0158	0.0903	0.0027	0.0071	0.0147	0.0733	0.0029
4	181	143	56	53	11	11	0.32	142	0.0037	0.0075	0.0603	0.0027	0.0035	0.0069	0.0517	0.0027
5	152	100	61	48	17	7	0.14	111	Model pruned							
6	145	121	84	58	19	6	0.15	109	Model pruned							
7	166	145	50	40	30	14	0.13	196	Model pruned							
8	131	91	56	52	16	10	0.47	125	0.0070	0.0140	0.0801	0.0027	0.0042	0.0083	0.0575	0.0027
9	106	124	104	43	16	9	0.18	84	Model pruned							
10	197	140	72	68	10	12	0.38	161	Model pruned							
11	176	111	95	57	38	8	0.27	149	Model pruned							
12	179	135	110	59	40	11	0.27	155	Model pruned							
13	166	158	76	51	33	9	0.34	96	Model pruned							
14	180	110	92	45	10	5	0.23	50	Model pruned							
15	166	132	66	63	25	15	0.37	140	Model pruned							
16	187	149	89	55	36	7	0.23	164	Model pruned							
17	200	130	79	40	27	12	0.3	120	Model pruned							
18	156	110	51	62	13	10	0.36	170	Model pruned							
19	134	147	110	53	24	8	0.42	141	Model pruned							
20	186	102	98	48	35	13	0.33	70	Model pruned							
21	138	83	60	52	13	10	0.5	128	Model pruned							
22	116	119	56	55	14	11	0.43	103	Model pruned							
23	118	82	56	48	21	9	0.5	120	Model pruned							
24	131	101	69	60	15	11	0.28	141	Model pruned							
25	161	116	62	55	11	6	0.41	90	Model pruned							
26	125	127	56	44	28	13	0.46	131	Model pruned							
27	174	137	73	51	19	8	0.35	113	Model pruned							
28	172	152	86	69	22	10	0.4	179	Model pruned							
29	144	95	105	65	18	13	0.36	132	Model pruned							

REFERENCES

[1] N. R. Council, M. S. Committee and others, Successful response starts with a map: improving geospatial support for disaster management, National Academies Press, 2007.

[2] I. Seeber, E. Bittner, R. O. Briggs, T. De Vreede, G.-J. De Vreede, A. Elkins, R. Maier, A. B. Merz, S. Oeste-Reiß, N. Randrup and others, "Machines as teammates: A research agenda on AI in team collaboration," *Information & management,* vol. 57, p. 103174, 2020.

[3] J. Laird, C. Ranganath and S. Gershman, "Future directions in human machine teaming workshop," *Arlington, VA: US Department of Defense,* 2020.

[4] N. J. McNeese, M. Demir, N. J. Cooke and C. Myers, "Teaming with a synthetic teammate: Insights into human-autonomy teaming," *Human factors,* vol. 60, p. 262–273, 2018.

[5] A. M. Madni and C. C. Madni, "Architectural framework for exploring adaptive human-machine teaming options in simulated dynamic environments," *Systems,* vol. 6, p. 44, 2018.

[6] C. Ong, K. McGee and T. L. Chuah, "Closing the human-AI team-mate gap: how changes to displayed information impact player behavior towards computer teammates," in *Proceedings of the 24th Australian Computer-Human Interaction Conference*, 2012.

[7] G. Bansal, B. Nushi, E. Kamar, W. S. Lasecki, D. S. Weld and E. Horvitz, "Beyond accuracy: The role of mental models in human-AI team performance," in *Proceedings of the AAAI conference on human computation and crowdsourcing*, 2019.

[8] C. Liang, J. Proft, E. Andersen and R. A. Knepper, "Implicit communication of actionable information in human-ai teams," in *Proceedings of the 2019 CHI conference on human factors in computing systems*, 2019.

[9] A. M. Turing, "Computing Machinery and Intelligence," *Mind,* vol. 59, p. 433–460, 1950.

[10] S. Hochreiter and J. Schmidhuber, "Long short-term memory," *Neural computation,* vol. 9, p. 1735–1780, 1997.

[11] Y. LeCun, L. Bottou, Y. Bengio and P. Haffner, "Gradient-based learning applied to document recognition," *Proceedings of the IEEE,* vol. 86, p. 2278–2324, 1998.

[12] B. E. Boser, I. M. Guyon and V. N. Vapnik, "A training algorithm for optimal margin classifiers," in *Proceedings of the fifth annual workshop on Computational learning theory*, 1992.

[13] J. E. McGrath, Groups: Interaction and performance, vol. 14, Prentice-Hall Englewood Cliffs, NJ, 1984.

[14] B. B. Morgan Jr, E. Salas and A. S. Glickman, "An analysis of team evolution and maturation," *The Journal of General Psychology,* vol. 120, p. 277–291, 1993.

[15] G. F. Goodwin, N. Blacksmith and M. R. Coats, "The science of teams in the military: Contributions from over 60 years of research.," *American Psychologist,* vol. 73, p. 322, 2018.

[16] J. Wenskovitch, C. Fallon, K. Miller and A. Dasgupta, "Beyond Visual Analytics: Human-Machine Teaming for AI-Driven Data Sensemaking," in *2021 IEEE Workshop on TRust and EXpertise in Visual Analytics (TREX)*, 2021.

[17] F. McCall, A. Hussein, E. Petraki, S. Elsawah and H. Abbass, "Towards a systematic educational framework for human-machine teaming," in *2021 IEEE International Conference on Engineering, Technology & Education (TALE)*, 2021.

[18] K. Holstein, V. Aleven and N. Rummel, "A conceptual framework for human–AI hybrid adaptivity in education," in *Artificial Intelligence in Education: 21st International Conference, AIED 2020, Ifrane, Morocco, July 6–10, 2020, Proceedings, Part I 21*, 2020.

[19] R. Eglash, L. Robert, A. Bennett, K. P. Robinson, M. Lachney and W. Babbitt, "Automation for the artisanal economy: enhancing the economic and environmental sustainability of crafting professions with human–machine collaboration," *Ai & Society,* vol. 35, p. 595–609, 2020.

[20] S. S. Sundar, "Rise of machine agency: A framework for studying the psychology of human–AI interaction (HAII)," *Journal of Computer-Mediated Communication,* vol. 25, p. 74–88, 2020.

[21] C. Flathmann, B. G. Schelble, P. J. Rosopa, N. J. McNeese, R. Mallick and K. C. Madathil, "Examining the impact of varying levels of AI teammate influence on human-AI teams," *International Journal of Human-Computer Studies,* vol. 177, p. 103061, 2023.

[22] M. Demir, N. J. McNeese and N. J. Cooke, "Understanding human-robot teams in light of all-human teams: Aspects of team interaction and shared cognition," *International Journal of Human-Computer Studies,* vol. 140, p. 102436, 2020.

[23] G. Zhang, L. Chong, K. Kotovsky and J. Cagan, "Trust in an AI versus a Human teammate: The effects of teammate identity and performance on Human-AI cooperation," *Computers in Human Behavior,* vol. 139, p. 107536, 2023.

[24] X. Puig, T. Shu, S. Li, Z. Wang, Y.-H. Liao, J. B. Tenenbaum, S. Fidler and A. Torralba, "Watch-and-help: A challenge for social perception and human-ai collaboration," *arXiv preprint arXiv:2010.09890,* 2020.

[25] S. Bhatti, M. Demir, N. J. Cooke and C. J. Johnson, "Assessing Communication and Trust in an AI Teammate in a Dynamic Task Environment," in *2021 IEEE 2nd International Conference on Human-Machine Systems (ICHMS)*, 2021.

[26] N. Donratanapat, S. Samadi, J. M. Vidal and S. S. Tabas, "A national scale big data analytics pipeline to assess the potential impacts of flooding on critical infrastructures and communities," *Environmental Modelling & Software,* vol. 133, p. 104828, 2020.

[27] P. Istalkar, A. Kadu and B. Biswal, "Value of process understanding in the era of machine learning: A case for recession flow prediction," *Journal of Hydrology,* p. 130350, 2023.

[28] G. Wee, L.-C. Chang, F.-J. Chang and M. Z. M. Amin, "A flood Impact-Based forecasting system by fuzzy inference techniques," *Journal of Hydrology,* vol. 625, p. 130117, 2023.

[29] M. Pourreza-Bilondi, S. Z. Samadi, A.-M. Akhoond-Ali and B. Ghahraman, "Reliability of semiarid flash flood modeling using Bayesian framework," *Journal of Hydrologic Engineering,* vol. 22, p. 05016039, 2017.

[30] R. J. Pally and S. Samadi, "Application of image processing and convolutional neural networks for flood image classification and semantic segmentation," *Environmental Modelling & Software,* vol. 148, p. 105285, 2022.

[31] C. W. Dawson and R. Wilby, "An artificial neural network approach to rainfall-runoff modelling," *Hydrological Sciences Journal,* vol. 43, p. 47–66, 1998.

[32] K. Thirumalaiah and M. C. Deo, "Hydrological forecasting using neural networks," *Journal of Hydrologic Engineering,* vol. 5, p. 180–189, 2000.

[33] P.-S. Yu, S.-T. Chen and I.-F. Chang, "Support vector regression for real-time flood stage forecasting," *Journal of hydrology,* vol. 328, p. 704–716, 2006.

[34] D. Han, L. Chan and N. Zhu, "Flood forecasting using support vector machines," *Journal of hydroinformatics,* vol. 9, p. 267–276, 2007.

[35] L. Windheuser, R. Karanjit, R. Pally, S. Samadi and N. C. Hubig, "An end-to-end flood stage prediction system using deep neural networks," *Earth and Space Science,* vol. 10, p. e2022EA002385, 2023.

[36] D. Liu, W. Jiang, L. Mu and S. Wang, "Streamflow prediction using deep learning neural network: case study of Yangtze River," *IEEE access,* vol. 8, p. 90069–90086, 2020.

[37] S. Nevo, E. Morin, A. Gerzi Rosenthal, A. Metzger, C. Barshai, D. Weitzner, D. Voloshin, F. Kratzert, G. Elidan, G. Dror and others, "Flood forecasting with machine learning models in an operational framework," *Hydrology and Earth System Sciences,* vol. 26, p. 4013–4032, 2022.

[38] *HURREVAC National Hurricane Program,* 2023.

[39] *FloodMap Mobile,* 2023.

[40] *Integrated Public Alert and Warning System,* 2023.

[41] W. Khan, A. Daud, K. Khan, S. Muhammad and R. Haq, "Exploring the frontiers of deep learning and natural language processing: A comprehensive overview of key challenges and emerging trends," *Natural Language Processing Journal,* p. 100026, 2023.

[42] F. Alam, U. Qazi, M. Imran and F. Ofli, "Humaid: human-annotated disaster incidents data from twitter with deep learning benchmarks," in *Proceedings of the International AAAI Conference on Web and Social Media*, 2021.

[43] G. Preda, *COVID19 X posts,* Kaggle, 2020.

[44] G. Preda, *Pfizer Vaccine X posts,* Kaggle, 2021.

[45] V. Stepanenko and I. Liubko, *Disaster X posts,* Kaggle, 2020.

[46] K. Suresh, *Bitcoin X posts,* Kaggle, 2021.

[47] D. A. V. I. D. WALLACH, *Financial X posts,* Kaggle, 2018.

[48] K. a. V. M. B. a. G. C. a. B. D. a. B. F. a. S. H. a. B. Y. Cho, "Learning phrase representations using RNN encoder-decoder for statistical machine translation," *arXiv preprint arXiv:1406.1078,* 2014.

[49] T. Akiba, S. Sano, T. Yanase, T. Ohta and M. Koyama, "Optuna: A next-generation hyperparameter optimization framework," in *Proceedings of the 25th ACM SIGKDD international conference on knowledge discovery & data mining*, 2019.

[50] A. D. Nobre, L. A. Cuartas, M. Hodnett, C. D. Rennó, G. Rodrigues, A. Silveira and S. Saleska, "Height Above the Nearest Drainage–a hydrologically relevant new terrain model," *Journal of Hydrology,* vol. 404, p. 13–29, 2011.

[51] Y. Liu, D. G. Tarboton and D. R. Maidment, "Height Above Nearest Drainage (HAND) and Hydraulic Property Table for CONUS," 2020.

[52] P. Huang, X. Lin, C. Liu, L. Fu and L. Yu, "A real-time automatic fire emergency evacuation route selection model based on decision-making processes of pedestrians," *Safety Science,* vol. 169, p. 106332, 2024.

[53] M. Rabbani, N. Oladzad-Abbasabady and N. Akbarian-Saravi, "Ambulance routing in disaster response considering variable patient condition: NSGA-II and MOPSO algorithms.," *Journal of Industrial & Management Optimization,* vol. 18, 2022.

[54] D. Y. Hancock, J. Fischer, J. M. Lowe, W. Snapp-Childs, M. Pierce, S. Marru, J. E. Coulter, M. Vaughn, B. Beck, N. Merchant and others, "Jetstream2: Accelerating cloud computing via Jetstream," in *Practice and Experience in Advanced Research Computing*, 2021, p. 1–8.

[55] M. Abadi, A. Agarwal, P. Barham, E. Brevdo, Z. Chen, C. Citro, G. S. Corrado, A. Davis, J. Dean, M. Devin and others, "Tensorflow: Large-scale machine learning on heterogeneous distributed systems," *arXiv preprint arXiv:1603.04467,* 2016.

[56] S. M. Idrees, M. A. Alam and P. Agarwal, "A prediction approach for stock market volatility based on time series data," *IEEE Access,* vol. 7, p. 17287–17298, 2019.